THE OHIO STATE UNIVERSITY

Analysis of Lossy Composite Terminating Structures

R. Andre, A. Dominek, J. Munk and N. Wang

The Ohio State University

ElectroScience Laboratory

Department of Electrical Engineering
Columbus, Ohio 43212

Technical Report 723224-3
Grant No. NAG3-1000
September 1991

National Aeronautics and Space Administration
Lewis Research Center
21000 Brookpark Rd.
Cleveland, OH 44135

NOTICES

When Government drawings, specifications, or other data are used for any purpose other than in connection with a definitely related Government procurement operation, the United States Government thereby incurs no responsibility nor any obligation whatsoever, and the fact that the Government may have formulated, furnished, or in any way supplied the said drawings, specifications, or other data, is not to be regarded by implication or otherwise as in any manner licensing the holder or any other person or corporation, or conveying any rights or permission to manufacture, use, or sell any patented invention that may in any way be related thereto.

50272-101

REPORT DOCUMENTATION PAGE	1. REPORT NO.	2.	3. Recipient's Accession No.

4. Title and Subtitle

Analysis of Lossy Composite Terminating Structures

5. Report Date

September 1991

6.

7. Author(s)

R. Andre, A. Dominek, J. Munk and N. Wang

8. Performing Org. Rept. No.

723224-3

9. Performing Organization Name and Address

The Ohio State University
ElectroScience Laboratory
1320 Kinnear Road
Columbus, OH 43212

10. Project/Task/Work Unit No.

11. Contract(C) or Grant(G) No.

(C)

(G) NAG3-1000

12. Sponsoring Organization Name and Address

National Aeronautics and Space Administration
Lewis Research Center
21000 Brookpark Rd., Cleveland, Ohio 44135

13. Report Type/Period Covered

Technical Report

14.

15. Supplementary Notes

16. Abstract (Limit: 200 words)

A finite element solution and computer code for the electromagnetic scattering of inhomogeneous penetrable bodies is presented. The application for the code is for the analysis and design of leading and trailing edge terminations when conducting and non-conducting materials are used. Examples of simple triangular shaped terminations are also presented.

17. Document Analysis a. Descriptors

MATERIALS
SCATTERING
MOMENT METHOD
RCS
2-D

b. Identifiers/Open-Ended Terms

c. COSATI Field/Group

18. Availability Statement

A. Approved for public release;
Distribution is unlimited.

19. Security Class (This Report)

Unclassified

20. Security Class (This Page)

Unclassified

21. No. of Pages

69

22. Price

(See ANSI-Z39.18) *See Instructions on Reverse* OPTIONAL FORM 272 (4-77)
Department of Commerce

Contents

Appendix

List of Figures

Chapter 1

Introduction

Leading and trailing edges on aerodynamic surfaces often have special edge terminations due to design constraints. One constraint is their impact upon the electromagnetic scattering performance for aerodynamic surfaces. The edges are important in determining the scattered field from these surfaces. Their impact is seen in several different ways. For an electrically thin, perfectly conducting surface, near grazing incidence, the leading edge is primarily sensitive to an electric field polarized parallel to the edge while the trailing edge is primarily sensitive to an electric field polarized perpendicular to the trailing edge.

The previously mentioned scattering behavior changes as the surface becomes electrically thicker. The leading edge becomes a specular scatterer and is sensitive to both polarizations while the trailing edge will allow energy to "creep" around the edge. Other changes occur when the surface is no longer perfectly conducting due to fabrication considerations. Now the incident field can penetrate the structure and scatter with greater complexity.

The character of the scattered field depends upon several parameters. The most important parameter is the shape of the structure. The scattered field

is focused in directions where Snell's law is satisfied. Backscattered fields are the strongest where the incident field direction is normal to a flat surface. A curved surface results in lower backscattered fields but then provides broader angular scattering. Hence, it is important to properly shape both the exterior and interior of penetrable surfaces.

Another parameter involves the various materials used in a penetrable surface. Abrupt changes in material with different electrical properties can also contribute to the scattered field. Thus, it is then desirable to taper the electrical material properties when possible. Appropriately chosen loss characteristics can also help in reducing the internal visibility of a structure when sufficient tapering is not possible.

Hence, the design of terminating structures involves the judicious choice of both structural shape and material components to achieve the desired electromagnetic scattering performance. A computer program is under development to assist in the design of two-dimensional edge terminations. This code is based upon the rigorous solution of Maxwell's equations.

The following chapters discuss the general formulation used in the code, its present status and a few examples to demonstrate the validity of the code. A future report will present the final form of the code, its operation and comparisons with measurements to illustrate particular design considerations for edge terminations.

Chapter 2

Theoretical Analysis

The analysis chosen for the basis of the computer program to calculate the scattered field from an edge termination was based upon its potential geometry and its material properties. Figure 2.1 illustrates a conceptual termination which has several homogeneous regions. Each region can be described geometrically with unique constitutive parameters. There are two basic approaches to solve such problems. The traditional approach involves the formulation of an integral equation with unknown equivalent volumetric currents occupying the space of the scatterer [1]. This approach is called a method of moments solution (MM) where the integral equation is discretized into a system of equations.

The alternate approach involves the direct solution of the differential form of Maxwell's equations [2, 3]. This approach is called a finite element solution. Traditional finite element solutions (FEM) have been employed in problems with bounded (finite) regions but their presence is becoming more common in problems with unbounded regions such as in electromagnetic scattering problems where the region extends to infinity.

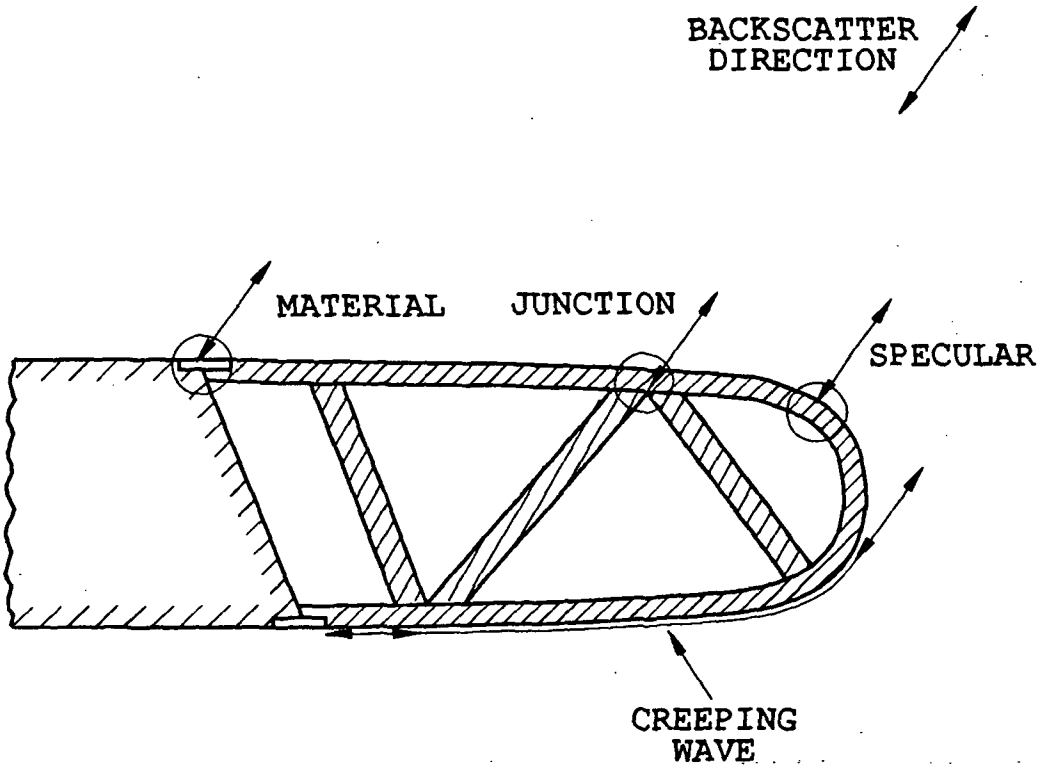

Figure 2.1: Illustration of conceptual edge termination.

There are several differences between the two basic approaches. The most noticeable difference involves the final matrix for inversion to solve for the unknowns. The MM solution yields a dense matrix while the FEM solution yields a sparse matrix. This difference becomes significant when the problem becomes electrically large since the number of unknowns will also increase. It is for this reason that the FEM approach was taken to develop the necessary scattering code.

The following sections briefly describe the FEM formulation and its implementation. The work is centered at determining the local and far fields from and inhomogeneous scatterer illuminated by a plane wave. The analysis is divided into two parts, i.e., the bounded internal region which consists of the scatterer and the unbounded external region which includes all of space excluding the scatterer.

I Interior Region

There are two independent scattered field solutions to Maxwell's equations for two dimensional geometries. Defining the geometry cross-section in the x-y plane, the solution is determined by the polarization of the incident field. The solution is called TM (transverse magnetic) if the incident electric field is $\hat{z}$ polarized or TE (traverse electric) if the incident magnetic field is $\hat{z}$ polarized. The scalar wave equation to be solved for the total field where the relative permittivity (ε_r) and permeability (μ_r) vary with position is

$$\nabla \cdot \left(\frac{1}{\nu}\nabla\phi\right) + \frac{1}{\nu}k^2\phi = 0 \tag{2.1}$$

where

$$\left.\begin{array}{rcl} \phi & = & E_z \\ \nu & = & \mu_r \end{array}\right\} \qquad \text{TM polarization.} \tag{2.2}$$

and

$$\left.\begin{array}{rcl} \phi & = & H_z \\ \nu & = & \epsilon_r \end{array}\right\} \qquad \text{TE polarization.} \tag{2.3}$$

with k being the propagation constant in the medium which equals $\frac{\omega}{c}\sqrt{\epsilon_r \mu_r}$. The total field is the sum of the incident and scattered fields denoted with superscripts i and s, respectively.

The total field solution can be obtained through using the technique of weighted residuals. This technique involves the integration of the differential equation over the bounded region S times a testing function, w_j. The resulting expression from this operation is

$$\int\int_S \frac{1}{\nu}\left(\nabla w_j \cdot \nabla \phi - \kappa^2 w_j \phi\right) dxdy = \int_{\partial\Gamma} \frac{w_j}{\nu}\frac{\partial \phi}{\partial n} dl \tag{2.4}$$

where we have made use of the vector identity

$$w_j \nabla \cdot \left\{\frac{1}{\nu}\nabla\phi\right\} = \nabla \cdot \left\{w_j \frac{1}{\nu}\nabla\phi\right\} - \frac{1}{\nu}\nabla w_i \cdot \nabla\phi. \tag{2.5}$$

The line integral is a result of applying the two dimensional divergence theorem to simplify Equation (2.4). This boundary term associated with $\partial\Gamma$, is dependent upon certain boundary conditions discussed later.

The next step is to expand ϕ in some basis and for simplicity, the same expansion as the testing function, w_j, is used for both. The expansion used are the common triangular elements [2] although there are several others.

The basis is a polynomial approximation represented by subsectional elements which span the bounded geometry region. The expanded region is represented with individual elements as shown below

$$\phi(x,y) = \sum_{e=1}^{N_e} \phi_e(x,y) \tag{2.6}$$

with each element, $\phi^e(x,y)$, being represented as

$$\phi^e(x,y) = \sum_{i=1}^{N_n} \phi_i w_i \tag{2.7}$$

where w_i are polynomial shape functions, N_e are the number of elements and ϕ_i represents the field at the ith node of the eth element. The constant N_n equals 3 or 6 depending upon if an element consists of three or six nodes as shown in Figure 2.2. A three nodal element corresponds to a linear approximation to the fields while a six nodal element allows a quadratic variation in the fields.

It is convenient to define the test functions such that $w_j = 0$ at all nodes except one, where it has unity value. This is accomplished by letting

$$w_i = R_i(n,\xi_1)R_j(n,\xi_2)R_k(n,\xi_3), \qquad i+j+k=n \tag{2.8}$$

where

$$\begin{aligned} R_m(n,\xi) &= \frac{1}{m!}\prod_{k=0}^{m-1}(n\xi - k), \qquad m > 0 \\ R_0(n,\xi) &= 1. \end{aligned} \tag{2.9}$$

The interpolation functions w_j may be expressed in terms of simplex coordinates which are independent of the global $x-y$ coordinates to simplify

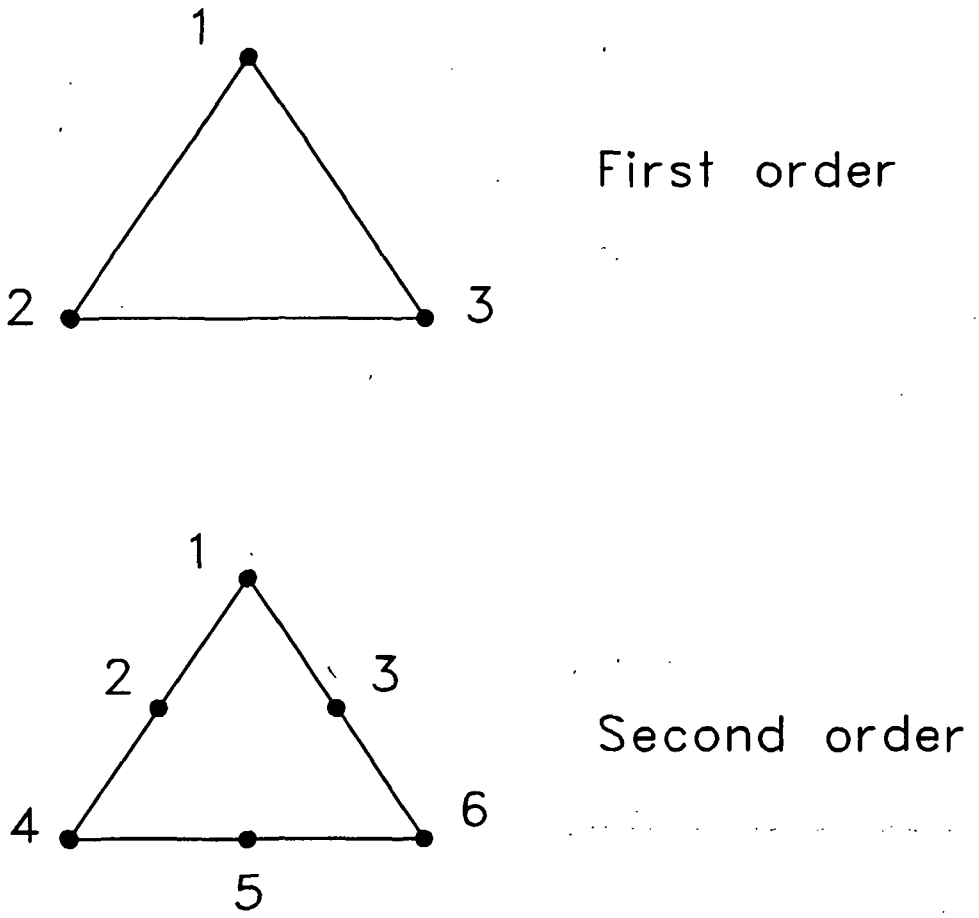

Figure 2.2: Typical first and second order triangular elements.

the necessary calculations [2]. The relationship between the cartesian and simplex coordinates is given by

$$\begin{bmatrix} \xi_1 \\ \xi_2 \\ \xi_3 \end{bmatrix} = \frac{1}{2A} \begin{bmatrix} x_2y_3 - x_3y_2 & y_2 - y_3 & x_3 - x_2 \\ x_3y_1 - x_1y_3 & y_3 - y_1 & x_1 - x_3 \\ x_1y_2 - x_2y_1 & y_1 - y_2 & x_2 - x_1 \end{bmatrix} \begin{bmatrix} 1 \\ x \\ y \end{bmatrix} \tag{2.10}$$

where

$$A = \frac{1}{2}\det \begin{bmatrix} 1 & x_1 & y_1 \\ 1 & x_2 & y_2 \\ 1 & x_3 & y_3 \end{bmatrix} \tag{2.11}$$

represents the area and x_1, y_1, x_2 etc... are the vertices of the element under consideration.

In matrix form, Equation (2.4), can be written as

$$\mathbf{Se} = \mathbf{v} \tag{2.12}$$

where

$$S_{ij} = \int\int_S \frac{1}{\nu} \left(\nabla w_i \cdot \nabla w_j - k^2 w_i w_j \right) dxdy \tag{2.13}$$

and

$$v_i = \frac{1}{\nu} \int_{\partial\Gamma} w_i \hat{n} \cdot \nabla\phi d\ell \tag{2.14}$$

Efficient evaluation of the terms in Equation (2.13) is provided in [2].

The final boundary consideration applies to conducting boundaries. The nodes along a conducting boundary are known for the TM case since $E_z^l = 0$ and are excluded from the matrix equation as unknowns. For the TE case, since the normal gradient is identically equal to zero along the conductor, the nodal points along the boundary are treated as unknowns.

II Exterior Region

The FEM approach allows a very convenient boundary condition implementation for bounded regions. However in scattering problems, the region is unbounded (boundary at infinity) and a far field boundary condition has to be employed. There are two basic approaches to accomplish this task. One approach is to construct a boundary near the scatterer which ideally absorbs all outward propagating waves and creates no reflected waves. This approach is called the absorbing boundary condition (ABC).

The second approach couples the fields calculated by a FEM calculation (bounded region) to the exterior through a integral expression provided by the boundary element method (BEM). This approach is called the hybrid FEM-BEM approach and is theoretically more accurate since no scattered field approximations are made at the coupling boundary as is done for the ABC method.

II.1 Absorbing Boundary Method

The goal in this technique is to make a bounded region from an unbounded region in order to directly use the FEM. This can be accomplished only approximately since the Sommerfeld far field radiation condition is only asymptotically satisfied at some boundary which encloses the scatterer. The Sommerfeld far field radiation condition

$$\lim_{\rho \to \infty} \frac{\partial \phi^s}{\partial \rho} = -jk\phi^s \tag{2.15}$$

is valid for $\partial\Gamma \rightarrow \infty$. However, for numerical analysis it is necessary to apply a boundary condition valid for $\partial\Gamma$ located at a finite distance from the

scatterer. From a practical standpoint, it should be as close as possible but far enough away for the following approximations to be valid.

Expanding the scattered field asymptotically

$$\phi^s(\rho,\theta) = \frac{e^{-jk\rho}}{\sqrt{\rho}}\left\{\phi_0(\theta) + \frac{\phi_1(\theta)}{\rho} + \frac{\phi_2(\theta)}{\rho^2} + \frac{\phi_3(\theta)}{\rho^3} + ...\right\}. \tag{2.16}$$

Imposing the Sommerfeld far field radiation condition on $\partial\Gamma$ results in only the first term of the asymptotic expansion being satisfied. Bayliss and Turkel [5] presented a higher order radiation condition

$$\frac{\partial\phi^s}{\partial\rho} = \alpha(\rho)\phi^s + \beta(\rho)\frac{\partial^2\phi^s}{\partial\theta^2} \tag{2.17}$$

which satisfies the first four terms in Equation (2.16), where

$$\alpha(\rho) = \left\{\frac{-jk - \frac{3}{2\rho} - \frac{j7}{8k\rho^2}}{1 - \frac{j}{k\rho}}\right\} \tag{2.18}$$

and

$$\beta(\rho) = \left\{\frac{\frac{-j}{2k\rho^2}}{1 - \frac{j}{k\rho}}\right\}. \tag{2.19}$$

Substituting Equation (2.17) into Equation (2.4) with $\phi^s = \phi - \phi^i$ and integrating-by-parts yields

$$\begin{aligned}
&\int\int_S \frac{1}{\nu}\left(\nabla w_j \cdot \nabla\phi - \kappa^2 w_j\phi\right) dxdy \\
&\quad - \int_{\partial\Gamma}\left(\alpha w_j\phi - \beta\frac{\partial w_j}{\partial\theta}\frac{\partial\phi}{\partial\theta}\right)\rho d\theta \\
&\quad = \int_{\partial\Gamma} w_j\left(\frac{\partial\phi^i}{\partial\rho} - \alpha\phi^i - \beta\frac{\partial^2\phi^i}{\partial\theta^2}\right)\rho d\theta
\end{aligned} \tag{2.20}$$

where $\partial\Gamma$ is circular and centered at the origin. In Equation (2.20), ϕ^i is assumed known while ϕ is the unknown variable.

In matrix form, Equation (2.20), can be written as

$$\mathbf{Se} = \mathbf{v}. \tag{2.21}$$

The matrix elements are given by

$$S_{ij} = S_{ij}^{A} + S_{ij}^{\ell} \tag{2.22}$$

where

$$S_{ij}^{A} = \int\int_{S} \frac{1}{\nu} \left(\nabla w_i \cdot \nabla w_j - k^2 w_i w_j \right) dxdy \tag{2.23}$$

$$S_{ij}^{\ell} = -\int_{\partial\Gamma} \left(\alpha w_i w_j - \beta \frac{\partial w_i}{\partial \theta} \frac{\partial w_j}{\partial \theta} \right) \rho d\theta \tag{2.24}$$

and

$$v_i = \int_{\partial\Gamma} w_i \left(\frac{\partial \phi^i}{\partial \rho} - \alpha \phi^i - \beta \frac{\partial^2 \phi^i}{\partial \theta^2} \right) \rho d\theta. \tag{2.25}$$

The terms expressed in Equation (2.23) have been previously computed, thus only the second integral need be considered. Due to limitations on the number of triangles one can expect to accommodate, approximating the curved boundary $\delta\Gamma$ by a straight line introduces discretization error. If, however, we do not restrict our trial function polynomials to exist only within the triangle but allow them to "spill" over onto the curved boundary we can eliminate this error [6]. This is valid since the polynomials exist over all space. The node values however, are still given at points on the triangle. In polar form the global coordinates are

$$\begin{bmatrix} \xi_1 \\ \xi_2 \\ \xi_3 \end{bmatrix} = \frac{1}{2A} \begin{bmatrix} x_2 y_3 - x_3 y_2 & y_2 - y_3 & x_3 - x_2 \\ x_3 y_1 - x_1 y_3 & y_3 - y_1 & x_1 - x_3 \\ x_1 y_2 - x_2 y_1 & y_1 - y_2 & x_2 - x_1 \end{bmatrix} \begin{bmatrix} 1 \\ \rho \cos\theta \\ \rho \sin\theta \end{bmatrix} \tag{2.26}$$

The test functions used in evaluating the integrals are the same functions previously given in Equation (2.8). Additionally, the partial derivatives in Equation (2.24) are expanded in terms of the area coordinates which yields

$$\frac{\partial w_i}{\partial \theta} = \sum_{i=1}^{3} \frac{\partial w_i}{\partial \xi_i} \frac{\partial \xi_i}{\partial \theta}. \tag{2.27}$$

Equation (2.24) is valid for a circular absorbing boundary centered at the origin of our coordinate system, therefore ρ is constant and Equation (2.24) can be solved in closed form.

Finally, the voltage coefficients v_i given in Equation (2.25) are considered. The incident plane wave with a e^{-jwt} time convention is used and is defined as

$$\phi^i(\rho, \theta) = \phi_0 e^{jk\rho\cos(\theta-\gamma)} \tag{2.28}$$

where ϕ_0 is the magnitude of the plane wave and γ is the angle of incidence. Taking the derivatives in Equation (2.25) results in

$$\frac{\partial \phi^i}{\partial \rho} = jk\cos(\theta-\gamma)\phi^i(\rho,\theta) \tag{2.29}$$

and

$$\frac{\partial^2 \phi^i}{\partial \theta^2} = \left\{-jk\rho\cos(\theta-\gamma) - k^2\rho^2\sin^2(\theta-\gamma)\right\}\phi^i(\rho,\theta). \tag{2.30}$$

Inserting Equations (2.29) and (2.30) into Equation (2.25) and numerically integrating yields the required coefficients, v_i.

II.2 Hybrid FEM/BEM

The efficiency of the FEM technique for unbounded problems can be greatly increased if the required meshed region can be reduced. The previously presented ABC technique allowed a convenient numerical approach at the cost of requiring many more unknowns in the region external to the scatterer. An alternate technique is to couple the internal FEM solution to the exterior, unbounded region through an integral equation formulation provided by the boundary element method (BEM) [7]. The BEM provides an efficient solution to the wave equation in a homogeneous region.

The FEM-BEM [8, 9, 10] method combines the strength of both of these methods. A single boundary is established at the surface of the material body. Inside the boundary, where the material properties may be inhomogeneous, the FEM solves for the fields. Outside the boundary, the BEM solution for free space is used which couples the incident field to the far field using the boundary conditions derived from the FEM. The link between the FEM and BEM is based on the boundary conditions of the differential equation at a discontinuity of the material properties. For electromagnetic fields, this reduces to continuity of tangential $\vec{E}$ and $\vec{H}$ across the surface of the material body.

This section will show how the FEM and the BEM are coupled together to solve for both the scattered far fields and the internal fields for an incident plane wave on an inhomogeneous two-dimensional body.

Differential Equation

The scattering problem being considered here is two dimensional. The material properties of the body are constant along the z axis and the incident field

is also constant in z. Under these conditions, Maxwell's equations separate into two equations which depend only on the values of the $\vec{E}, \vec{H}$ fields in the $\hat{z}$ direction,

$$\left(\nabla \cdot (\frac{1}{\mu_r} \nabla E_z) + \frac{k^2}{\mu_r} E_z\right) = 0 \tag{2.31}$$

and

$$\left(\nabla \cdot (\frac{1}{\varepsilon_r} \nabla H_z) + \frac{k^2}{\varepsilon_r} H_z\right) = 0. \tag{2.32}$$

The relative permittivity ε_r, permeability μ_r, and wave number $k = \frac{\omega}{c}\sqrt{\mu_r \varepsilon_r}$ may depend on position x, y. The derivative ∇ is in the x, y direction only. The other field components may be derived from E_z and H_z.

For a transverse magnetic (TM) field,

$$\vec{E}_{inc} = E_0 \hat{z} e^{-j\vec{k}_i \cdot \vec{\rho}} \tag{2.33}$$

and the scattered field will also be TM. Likewise a transverse electric (TE) incident field,

$$\vec{H}_{inc} = H_0 \hat{z} e^{-j\vec{k}_i \cdot \vec{\rho}} \tag{2.34}$$

will produce only TE scattered fields. Both the TE and TM differential equations have the form of the scalar equation

$$\left(\nabla \cdot (\frac{1}{\nu} \nabla \phi) + \frac{k^2}{\nu} \phi\right) = 0 \tag{2.35}$$

with an incident field defined as

$$\phi_{inc} = \phi_0 e^{-j\vec{k}_i \cdot \vec{\rho}}. \tag{2.36}$$

This scalar equation is the differential equation which will be solved by the FEM-BEM with the understanding that the solution corresponds to either the TM case with $\phi = E_z, \nu = \mu_r$ or to the TE case with $\phi = H_z, \nu = \varepsilon_r$.

Boundary Conditions

At a boundary between material 1 and material 2 with parameters ν_1, k_1 and ν_2, k_2 respectively, the differential equation provides the following boundary conditions,

$$\phi_1 = \phi_2 \tag{2.37}$$

$$\frac{1}{\nu_1}\frac{\partial \phi_1}{\partial n} = \frac{1}{\nu_2}\frac{\partial \phi_2}{\partial n} \tag{2.38}$$

where $\hat{n}$ is an outward unit vector normal to the boundary and $\frac{\partial}{\partial n}$ is a derivative in the $\hat{n}$ direction. The last boundary condition can be written

$$\psi_1 = \psi_2 \tag{2.39}$$

$$\psi = \frac{1}{\nu}\frac{\partial \phi}{\partial n}. \tag{2.40}$$

The fields ϕ and ψ are continuous across the boundary.

Let $\hat{t} = \hat{z} \times \hat{n}$ be a unit vector tangential to the surface. Then for TM fields

$$\phi = E_z \tag{2.41}$$

$$\psi = j\omega \hat{t} \cdot \vec{H} \tag{2.42}$$

and for TE fields

$$\phi = H_z \tag{2.43}$$

$$\psi = -j\omega \hat{t} \cdot \vec{E}. \tag{2.44}$$

The boundary conditions on ϕ and ψ are equivalent to enforcing continuity of tangential $\vec{E}$ and $\vec{H}$.

FEM

The FEM is ideal for solving the differential equation shown in Equation (2.35). To construct a solution, a mesh of triangular elements is made which completely encloses the material body. As usual this mesh is made small enough to accurately model the inhomogeneity of the body and the variation of the fields. Nodes on the edges of the triangles represent the value of ϕ at that point. These nodal values are used to extrapolate a linear or quadratic solution in the element. Each node i gives rise to a generating function w_i which extends across each element node i touches, has unit value at node i and has zero value at every other node. The total field can be written as a linear combination of these generating functions,

$$\phi = \sum_{i=1}^{N} \phi_i w_i \tag{2.45}$$

where ϕ_i is the value at node i for the N nodes on the mesh.

The FEM solution seeks to minimize the residual of the differential equation as weighted by each generating function w_j. The residual for the jth generating function is

$$R_j = -\int_S \left(\nabla \cdot (\frac{1}{\nu} \nabla \phi) + \frac{k^2}{\nu} \phi \right) w_j ds. \tag{2.46}$$

After an integration by parts, this residual becomes,

$$R_j = -\int_S \frac{1}{\nu} \left(\nabla w_j \cdot \nabla \phi - k^2 w_j \phi \right) ds + \int_C w_j \psi dl. \tag{2.47}$$

The region of integration is S which is enclosed by the boundary C. The FEM boundary coincides with C. As before, $\psi = \frac{1}{\nu}\frac{\partial \phi}{\partial n}$ on the boundary and is assumed independent (known). There are N residual equations. Using the expansion in Equation (2.45) for ϕ and setting the residuals to zero gives N equations in the N unknowns ϕ_i,

$$\int_C w_j \psi dl = \sum_{i=1}^{N} \phi_i \int_S \frac{1}{\nu} \left(\nabla w_j \cdot \nabla w_i - k^2 w_j w_i \right) ds. \tag{2.48}$$

This is the matrix equation,

$$V_j = S_{ji}\phi_i \tag{2.49}$$

$$S_{ji} = \int_S \frac{1}{\nu} \left(\nabla w_j \cdot \nabla w_i - k^2 w_j w_i \right) ds \tag{2.50}$$

$$V_j = \int_C w_j \psi dl \tag{2.51}$$

with S_{ji} an $N \times N$ matrix and V_j an N dimensional vector. There is an implied summation over repeated indices in this and the following matrix equations.

For a node k on the boundary, there is a generating function w_k^B, restricted to the boundary, which has unit value at node k and is zero at all other boundary nodes. These generating functions provide a means for expanding ψ on the boundary,

$$\psi = \sum_{i=1}^{N_B} \psi_k w_k^B \tag{2.52}$$

in terms of ψ_k, the value of ψ at the kth boundary node. The total number of boundary nodes is N_B. Substituting this expansion for ψ into the formula for V_j gives the matrix equation,

$$V_j = T_{jk}\psi_k \tag{2.53}$$

$$T_{jk} = \int_C w_j w_k^B dl \tag{2.54}$$

where T_{jk} is a nonsquare matrix with N rows and N_B columns. The FEM matrix equation becomes,

$$T_{jk}\psi_k = S_{ji}\phi_i. \tag{2.55}$$

Inverting the FEM matrix S_{ji} and solving for ϕ_i gives,

$$\phi_i = \left(S^{-1}\right)_{ij} T_{jk}\psi_k. \tag{2.56}$$

This equation gives the internal field ϕ in terms of ψ, the normal derivative of ϕ on the boundary. Note that the index i runs from 1 to N for the total number of nodes while k runs from 1 to N_B for the boundary nodes. For the linkage to the BEM, ϕ need only be known on the boundary. We therefore restrict i to these boundary nodes with the index k' which runs from 1 to N_B.

$$\phi_{k'} = I_{k'k}\psi_k \tag{2.57}$$

$$I_{k'k} = \left(S^{-1}\right)_{k'j} T_{jk}. \tag{2.58}$$

The matrix $I_{k'k}$ is a square $N_B \times N_B$ matrix which relates ϕ on the boundary to ψ on the boundary. This matrix acts like an impedance boundary condition and will be used as part of the BEM solution.

In the formula for the impedance matrix, the inverse of the FEM matrix S_{ji} is shown. Finding this inverse is not necessary. The matrix S_{ji} is banded and large so that taking the inverse could be very costly. Given a value of

ψ on the boundary, the solution of ϕ throughout the internal region and on the boundary can be obtained quickly using matrix algorithms for banded matrices. The mth column of the impedance matrix is therefore obtained by setting $\psi_m = 1$ and $\psi_k = 0$ for $k \neq m$ and solving for $\phi_{k'}$. The mth column of the impedance matrix is then given by,

$$I_{k'm} = \phi_{k'}. \tag{2.59}$$

This method requires N_B iterations to build the N_B columns of $I_{kk'}$.

BEM

The BEM is an integral equation method for solving fields in a homogeneous region. This integral equation is reduced using moment method techniques to a matrix equation which relates the known incident field to a set of unknown coefficients. Solution of the matrix equation solves for the unknown coefficients and from these coefficients, the scattered field may be determined.

Consider a region S bounded by the curve C. This time, however, the area exterior to S will be included in the analysis. Because the exterior region is free space and homogeneous, $\nu^+ = 1$ and $k^+ = k_0 = \frac{\omega}{c}$. The superscript $+$ refers to the exterior region. Inside S, the parameters ν^- and k^- may vary.

The integral equation is usually derived from Green's second identity which yields the following relation for the field ϕ exterior to S in terms of the value of ϕ and ψ on the boundary curve C,

$$\phi = \phi_{inc} - \int_C G_0(\vec{\rho}, \vec{\rho'})\nu^+\psi(\vec{\rho'}) - \frac{\partial G_0(\vec{\rho}, \vec{\rho'})}{\partial n'}\phi(\vec{\rho'})dl'. \tag{2.60}$$

The outward normal is $\hat{n'}$ and $\frac{\partial}{\partial n'}$ is the derivative along the normal. Since ϕ and ψ are continuous across a material boundary, no superscript is needed

to distinguish the interior and exterior fields. The Green's function solution for the two dimensional wave equation in free space is,

$$G_0(\vec{\rho},\vec{\rho'}) = \frac{-j}{4} H_0^{(2)}(k_0\|\vec{\rho}-\vec{\rho'}\|). \tag{2.61}$$

The zeroth order Hankel function of the second kind is consistent with the $e^{j\omega t}$ time convention.

This integral relation is valid everywhere in the exterior region and can be used to find the far field once ϕ and ψ are known. The integral equation results from taking the field point on the boundary. Rearranging terms,

$$\begin{aligned}\phi_{inc} &= \left[\int_C G_0(\vec{\rho},\vec{\rho'})\nu^+\psi(\vec{\rho'})dl'\right] \\ &\quad + \left[\phi - \int_C \frac{\partial G_0(\vec{\rho},\vec{\rho'})}{\partial n'}\phi(\vec{\rho'})dl'\right].\end{aligned} \tag{2.62}$$

This equation relates the unknown ϕ and ψ on the boundary in terms of the known incident field ϕ_{inc}. Substituting the expansion of ϕ and ψ on the basis of boundary weighting functions into this integral equation,

$$\begin{aligned}\phi_{inc} &= \sum_{k=1}^{N_B}\psi_k\left[\int_C G_0(\vec{\rho},\vec{\rho'})\nu^+ w_k^B(\vec{\rho'})dl'\right] \\ &\quad + \sum_{k'=1}^{N_B}\phi_{k'}\left[w_{k'}^B - \int_C \frac{\partial G_0(\vec{\rho},\vec{\rho'})}{\partial n'} w_{k'}^B(\vec{\rho'})dl'\right].\end{aligned} \tag{2.63}$$

The moment method testing functions are chosen to be the boundary weighting functions w_j^B. This gives a Galerkin form of moment method solution since the expansion and testing functions are the same. Applying each of these testing functions to the integral equation gives the matrix equation,

$$V_j = M_{jk}^{\psi+}\psi_k + M_{jk'}^{\phi+}\phi_{k'} \tag{2.64}$$

where

$$V_j = \int_C w_j^B \phi_{inc} dl' \tag{2.65}$$

$$M_{jk}^{\psi+} = \nu^+ \int_C \int_C w_j^B(\vec{\rho}) G_0(\vec{\rho}, \vec{\rho}') w_k^B(\vec{\rho}') dl' dl \tag{2.66}$$

$$M_{jk'}^{\phi+} = \int_C \int_C w_j^B w_{k'}^B dl' dl - \int_C \int_C w_j^B(\vec{\rho}) \frac{\partial G_0(\vec{\rho}, \vec{\rho}')}{\partial n'} w_{k'}^B(\vec{\rho}') dl' dl \tag{2.67}$$

The matrices $M_{jk}^{\psi+}$, $M_{jk'}^{\phi+}$ are $N_B \times N_B$ square matrices. $M_{jk}^{\psi+}$ is symmetric, but $M_{jk'}^{\phi+}$ is not. There are N_B equations and $2N_B$ unknowns in this matrix equation. Another set of N_B equations is needed to complete the solution.

So far no information about the interior region has been used. If the interior is homogeneous, another integral equation can be derived which depends on the value of ϕ and ψ on the boundary and uses the interior Green's function solution with parameters ν^-, k^-. This provides another N_B set of equations in the $2N_B$ unknowns, $\phi_{k'}$ and ψ_k. Simultaneous solution of the resulting $2N_B$ equations gives the BEM solution for the scattering from a homogeneous dielectric body. The far field may be found using Equation (2.60) along with the asymptotic form of the Hankel function,

$$\begin{aligned} \phi_{far}(\hat{\rho}\rho) \;=\; & \frac{e^{-jk_0\rho}}{\sqrt{\rho}} \left(\frac{j}{4} \sqrt{\frac{2j}{\pi k_0}} \right) \left[\sum_{k=1}^{N_B} \psi_k \nu^+ \int_C w_k^B(\vec{\rho}') e^{jk_0 \hat{\rho} \cdot \vec{\rho}'} dl' \right. \\ & \left. + \sum_{k'=1}^{N_B} \phi_{k'} \int_C -jk_0 (\hat{n}' \cdot \hat{r}) w_{k'}^B(\vec{\rho}') e^{jk_0 \hat{\rho} \cdot \vec{\rho}'} dl' \right] \end{aligned} \tag{2.68}$$

This equation gives the far field ϕ in the $\hat{\rho}$ direction in terms of the boundary fields at the nodal points $\phi_{k'}$,ψ_k.

For an inhomogeneous body, additional internal boundaries can be included and corresponding integral equations derived. The number of unknowns grows rapidly and can quickly become unmanageable. What is needed by the BEM is an additional relation between ϕ and ψ on the boundary. This is exactly what the FEM interior solution provides.

FEM-BEM

The FEM and BEM are combined by substituting the impedance matrix Equation (2.58) derived from the FEM into the BEM matrix Equation (2.64). This operation uses the continuity of ϕ and ψ across the boundary curve C. The result is

$$V_j = A_{jk}\psi_k \tag{2.69}$$

$$A_{jk} = M^{\psi+}_{jk} + M^{\phi+}_{jk'} I_{k'k}. \tag{2.70}$$

The unknowns in this matrix equation are the values of ψ on the boundary. The solution for ψ_k,

$$\psi_k = \left(A^{-1}\right)_{kj} V_j \tag{2.71}$$

depends on the incident field through V_j. The matrix A_{jk} is independent of the incident field.

Once the ψ_k are known, the internal field ϕ may be found by solving the FEM matrix Equation (2.56) with the known values of ψ_k. The impedance matrix is used to find the boundary value of ϕ as in Equation (2.58). The field can then be found in the far field by using Equation (2.68) and the ϕ, ψ boundary values.

III Matrix Inversion

The resulting system of equations to be solved involves the inversion of a square matrix. This matrix is very sparse due to the limited coupling between elements. The location of non-zero elements in the matrix is dependent

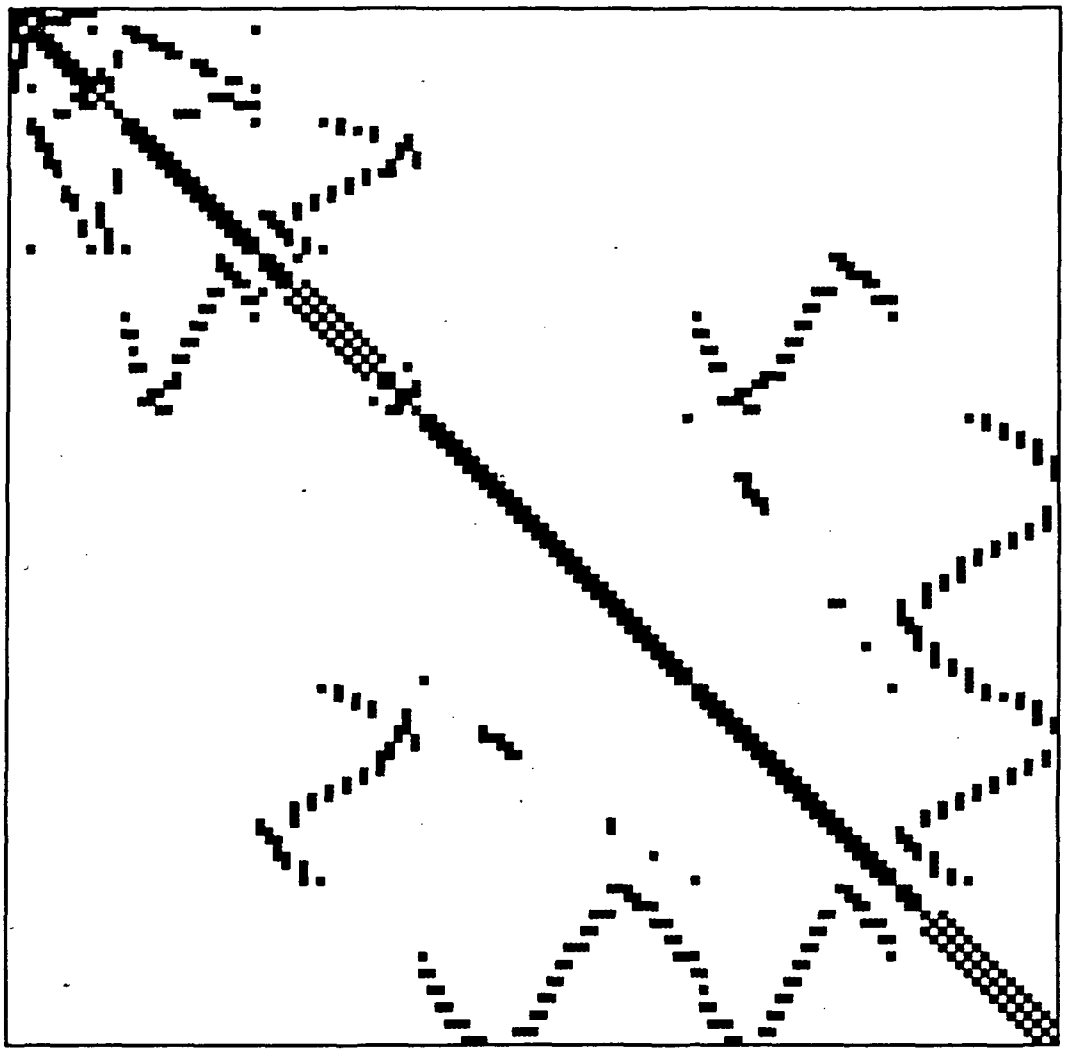

Figure 2.3: Matrix distribution of non-zero elements before renumbering.

upon the nodal numbering. Numbering of the nodes should be done to always minimize the difference of neighboring nodes. This allows the matrix to become very banded for greater inversion and internal memory storage efficiency.

Presently, a renumbering algorithm [12] is used to renumber the nodes. Figures 2.3 and 2.4 demonstrate the element distribution of a typical matrix composed with 123 nodes before and after the renumbering, respectively. The darkened squares represent non-zero elements. Note that the bandwidth of

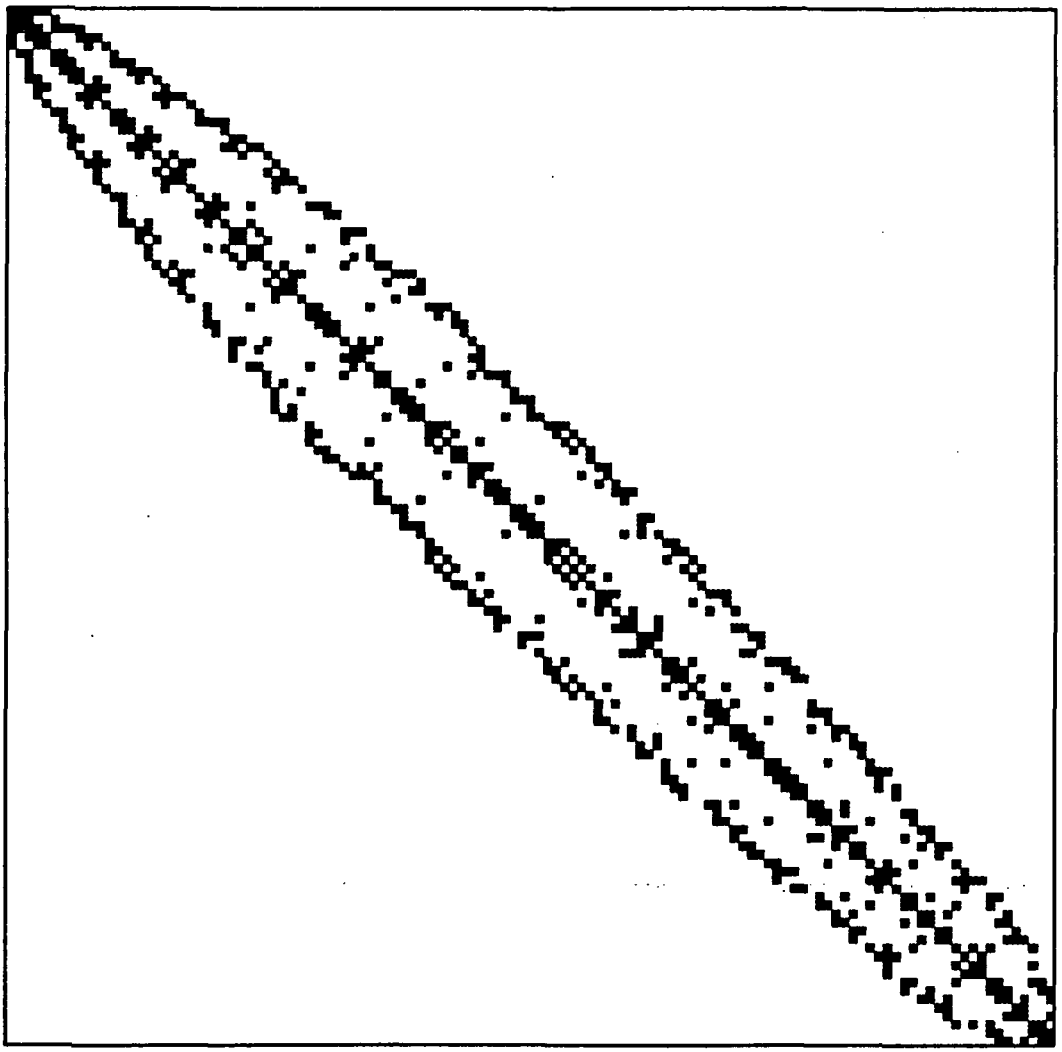

Figure 2.4: Matrix distribution of non-zero elements after renumbering.

the matrix is dramatically reduced. The initial and final bandwidth was 70 and 17, respectively for this particular matrix. The bandwidth is defined here to be the maximum difference minus one of the non-zero matrix elements for any row.

The actual solver used employs simple Gaussian elimination to obtain the unknown nodal values. This appears to be adequate when the elements have approximately the same area size. When there is a drastic difference between element size, a partial pivoting algorithm would be required. However, this requirement would require more storage than presently used since only the banded elements of the matrix are stored.

IV Scattered Far Fields

Although the FEM solution provides fields in the vicinity of the scattering geometry, most often the scattered far field is of interest. A useful normalization quantity for the scattered far field is the echo width as defined below:

$$\text{Echo Width} = 2\pi \lim_{\rho \to \infty} \rho \frac{\|U^s\|^2}{\|U^i\|} \tag{2.72}$$

where U^s represents the scattered field for either polarization.

Obtaining the scattered far field for the ABC and BEM approaches is slightly different. The ABC approach uses the calculated total field at some specified circular boundary. The scattered field can be represented as

$$U^s = \sum_{n=-\infty}^{\infty} a_n j^{-n} H_n^2(\kappa\rho) e^{jn\phi} \tag{2.73}$$

where a_n are coefficients and H_n^2 are Hankel functions of the second kind. Once the coefficients are found, the scattered far field is obtained by using

the large argument form for the Hankel function. The scattered far field is then given by

$$U^s = \sum_{n=-\infty}^{\infty} a_n \sqrt{\frac{2j}{\pi\lambda}} e^{jn\phi} \frac{e^{-j\kappa\rho}}{\sqrt{\rho}}. \tag{2.74}$$

The coefficients a_n are determined by the following expression, independent upon how the total fields, U^t, are calculated:

$$a_n = \frac{j^n \frac{1}{2\pi} \int_0^{2\pi} U^t(a,\phi) e^{jn\phi} d\phi - (-1)^n J_n(\kappa a) e^{jn\phi^i}}{H_n^2(\kappa a)} \tag{2.75}$$

where U^t is the total field at $\rho = a$ and J_n is a Bessel function. The integration in this equation yields the nth order contribution for the scattered and incident fields. The scattered field is then obtained by subtracting the nth order incident field (plane wave) contribution from the nth order total field.

The BEM approach instead uses equivalent currents which are calculated at the coupling boundary surrounding the scatterer. The fields from these currents are then radiated into the far field using the standard radiation integral as discussed earlier.

V Geometry Specification

For any numerical solution, the geometry under consideration has to be specified. The approach chosen here is to use a commercially available CAD package and mesher to provide the scattering code required data. Several packages are available at very reasonable costs. The package chosen here is provided by Structural Research and Analysis Corporation [4] and is called Geostar. They have implementations available on several computers ranging from PC's to workstations.

The scattering code reads an ASCII output file generated by Geostar which describes the geometry in terms of first or second order triangular elements. This file lists the coordinates of the nodes, the global node numbering for each element, material specification for each element and required information to enforce the necessary boundary conditions.

Chapter 3

Examples

Two different example classes are presented. One is to validate the computer solution through comparisons with results generated by eigenfunction solutions. The other examines the scattered fields from some simple terminations. The calculated results shown here were all obtained using the FEM/BEM approach. The FEM/ABC appears not as robust and requires a much greater mesh and hence more unkowns. The greater number of unknowns may not be as significant interms of compution time and required storage as the error resulting from the field propagating through the extra mesh. It is desirable to keep the meshed area as small as possible to minimize discretization error. Hence, the FEM/BEM is a natural for this. A future report will document the FEM/ABC performance.

I Validation

Code validation usually results through the comparison of its calculations to measurements or calculations through other independent solutions. An eigenfunction solution is considered to be the most exact form of numerical solution available. For this validation, comparisons will be made to two

Table 3.1: Geometry data

Geometry	Nodes	Elements	Bandwidth	Run Time (s)
Con-Cylinder	1577	3016	52	126
Strip	90	120	9	3.2
Termination 1	2087	3873	45	387
Termination 2	2087	3873	45	393
Termination 3	1652	3030	41	280

geometries where eigenfunction solutions exist. The validation geometries will be (1) two concentric dielectric cylinders and (2) a perfectly conducting flat strip. The excitation in both cases will be from plane wave incidence as illustrated in Figure 3.1.

The dimensions for the dielectric cylinder are 7 and 16 cm for the inner and outer radii, respectively. The relative permittivities for the inner and outer regions are $\epsilon_r = (4., -j.2)$ and $\epsilon_r = (2., -j.1)$. The relative permeability for both regions is unity. The width for the strip geometry is 10 cm. The frequency of the incident field for both cases is 3 GHz. The meshed geometries are illustrated in Figures 3.2 and 3.3. The mesh density used for both cases was approximately 10 nodes per linear length per free space wavelength. The BEM boundary was located at the perimeter of the meshed regions. Table I contains mesh information and computer run time for all the geometries.

Figures 3.4 and 3.5 compare the TE and TM, respectively, FEM/BEM and eigenfunction bistatic echo width solutions for the concentric dielectric cylinders. Figures 3.6 and 3.7 compare the TE and TM, respectively, FEM/BEM and eigenfunction monostatic echo width solutions for the flat strip. All calculations used linear shape functions. Agreement between the

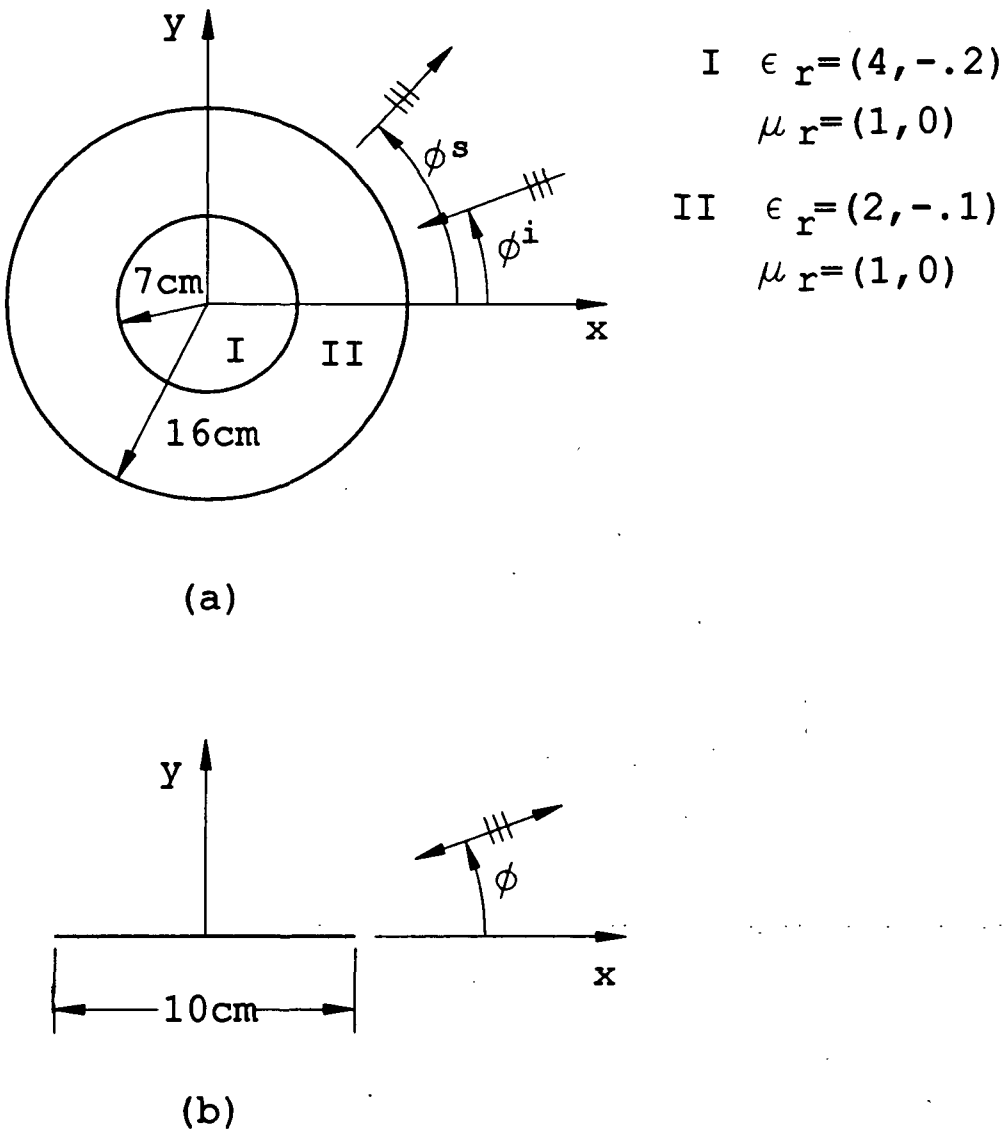

Figure 3.1: Test geometries: (a) Concentric cylinders, (b) Flat strip.

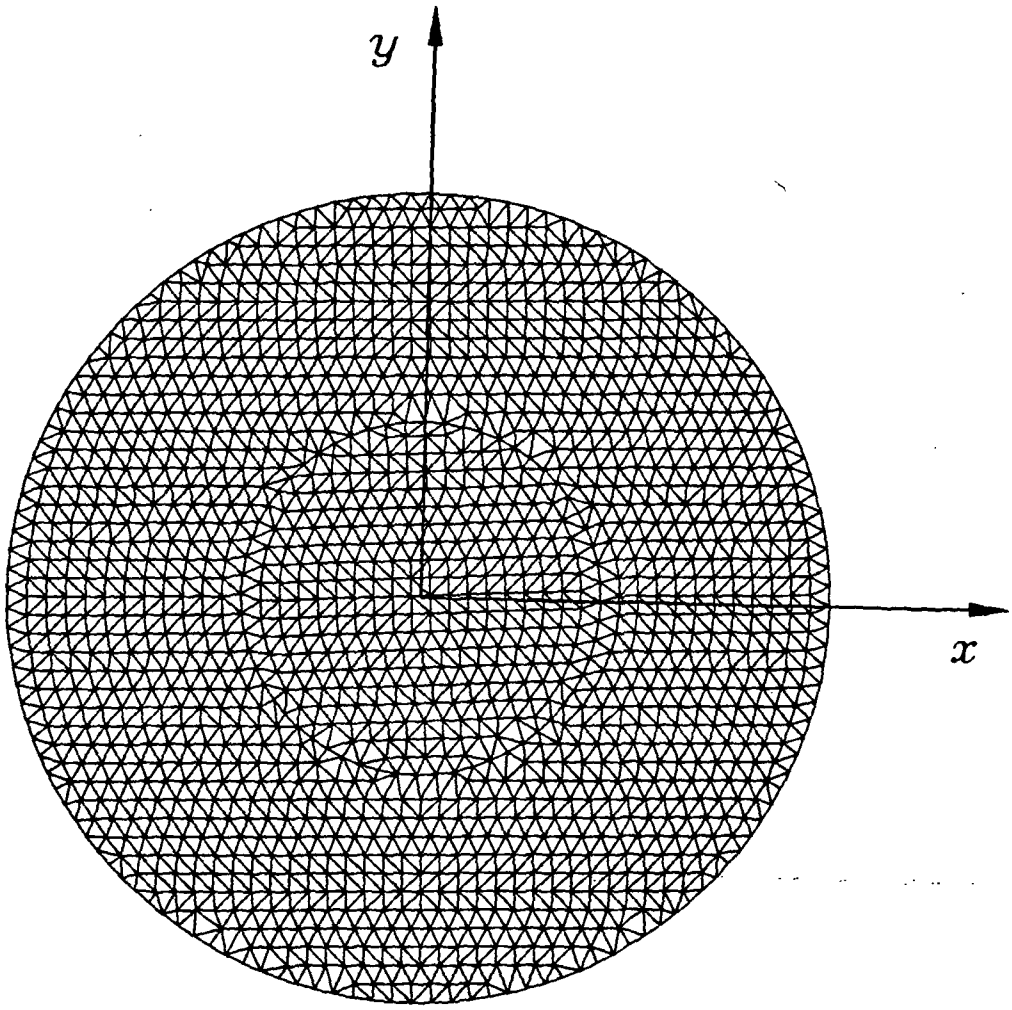

Figure 3.2: Mesh used for the concentric cylinders.

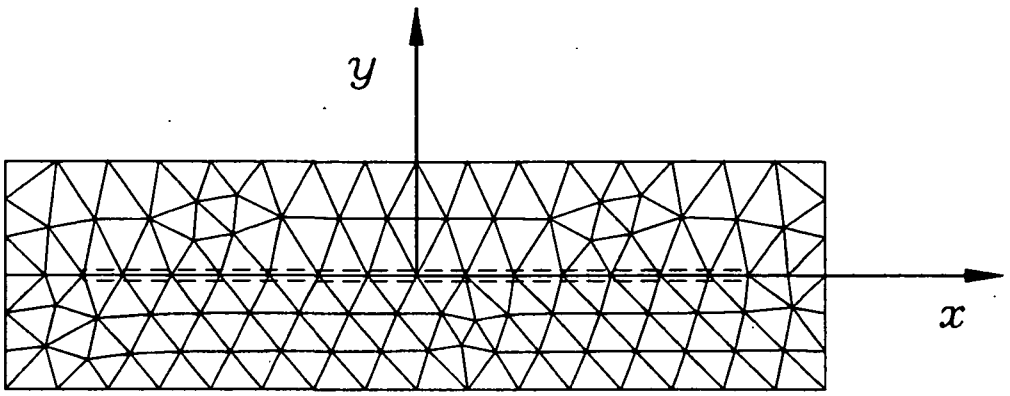

Figure 3.3: Mesh used for the flat strip. The centerline of the dashed region is the location of the strip.

eigenfunction and FEM/BEM results improve as the mesh density is increased and/or higher order expansion functions are used.

II Terminations

Three examples are shown here to demonstrate simple triangular terminations. The terminations are lossy dielectric structures with a conducting backplane and are designated as T1, T2 and T3. Terminations T1 and T2 are shown in Figure 3.8a. and termination T3 is shown in Figure 3.8b. The relative dielectric constant for termination T1 had a uniform value of $\epsilon_r = (4., -.05)$. Termination T2 had its relative dielectric constant linearly graded from $\epsilon_r = (2., -.05)$ at its tip to $\epsilon_r = (4., -.2)$ at its base. The relative dielectric constant for termination T3 had a uniform value of $\epsilon_r = (4., -.05)$. The relative permbeality for all three cases was $\mu = (1., 0.)$.

Figures 3.9 through 3.11 contain the TM and TE echo widths for terminations T1 through T3, respectively. All calculations were performed at 3 GHz with a linear nodal density of 20 per material wavelength.

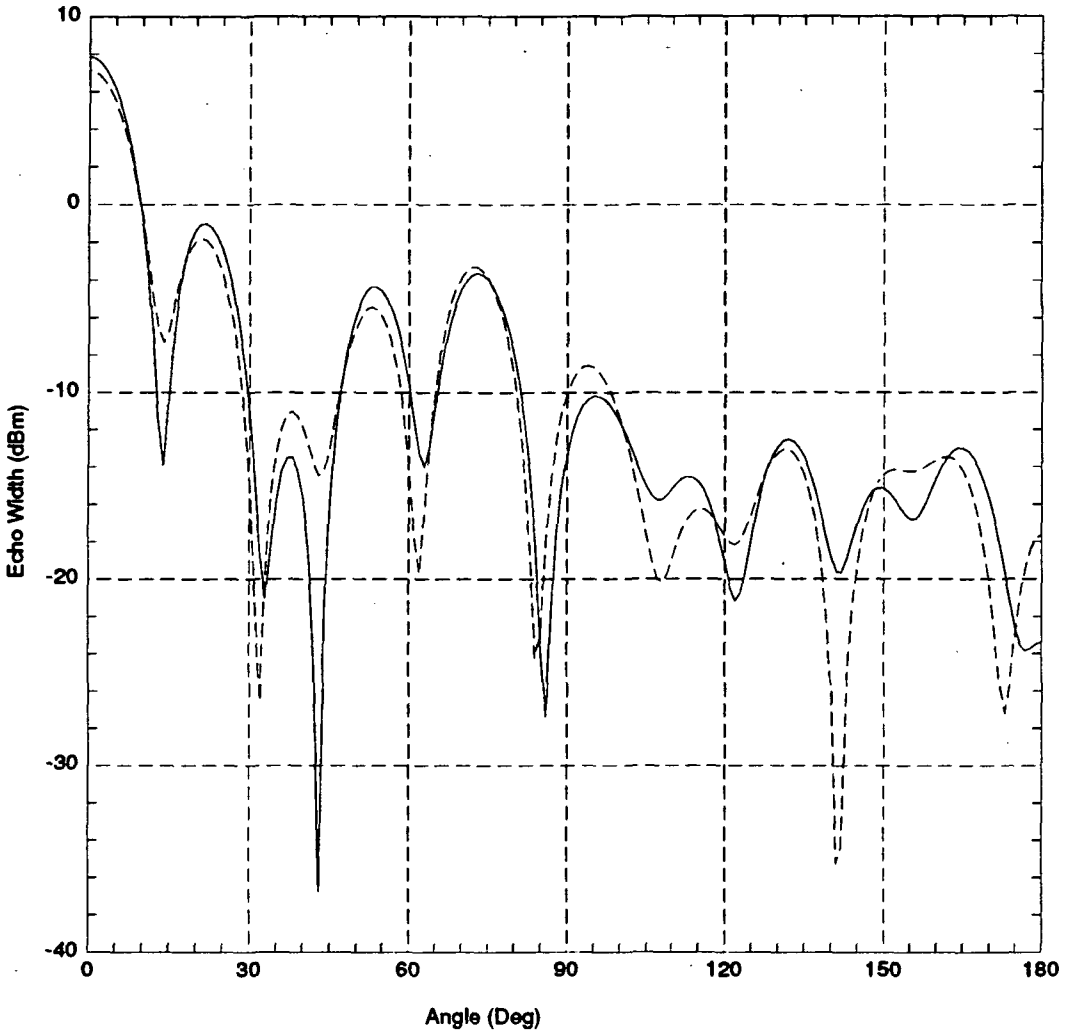

Figure 3.4: TM bistatic echo width for the dielectric concentric cylinders. FEM/BEM - solid, Eigenfunction - dashed.

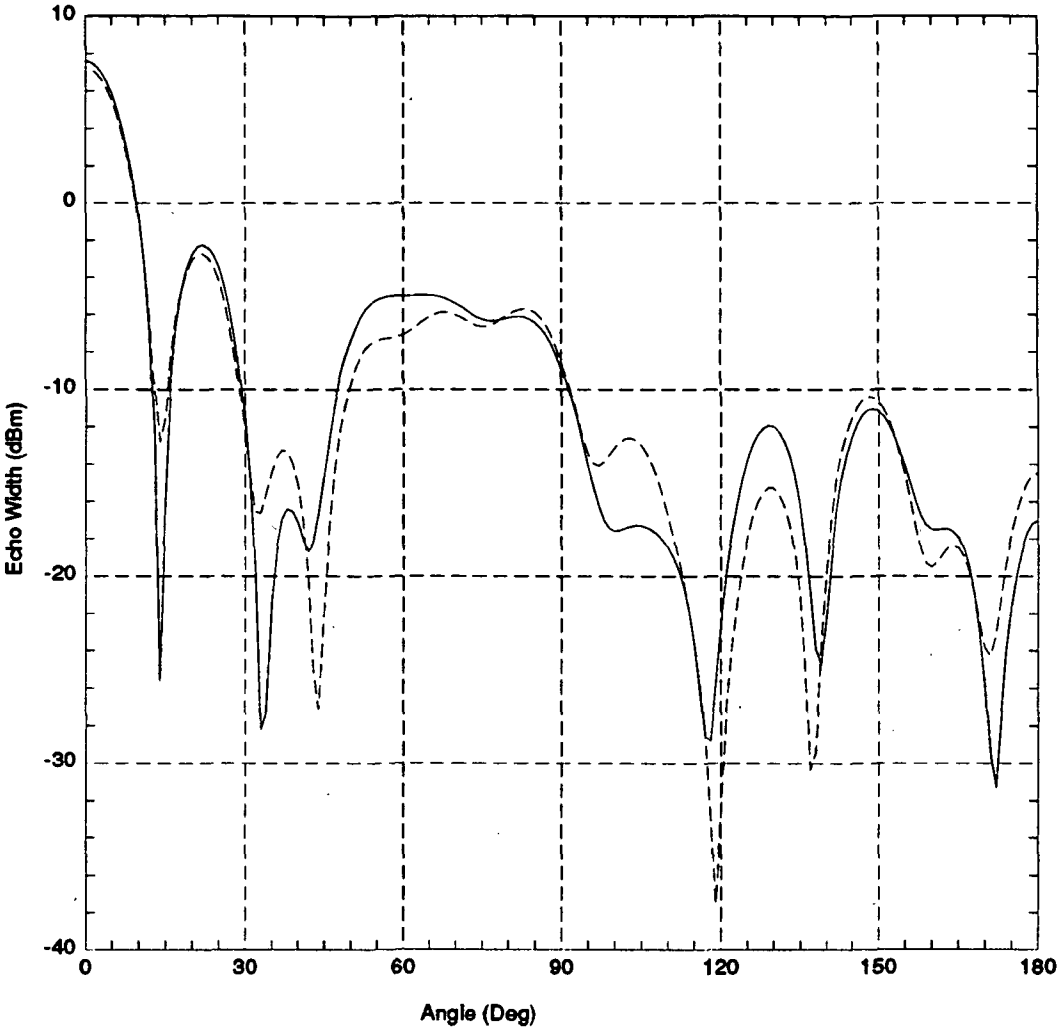

Figure 3.5: TE bistatic echo width for the dielectric concentric cylinders. FEM/BEM - solid, Eigenfunction - dashed.

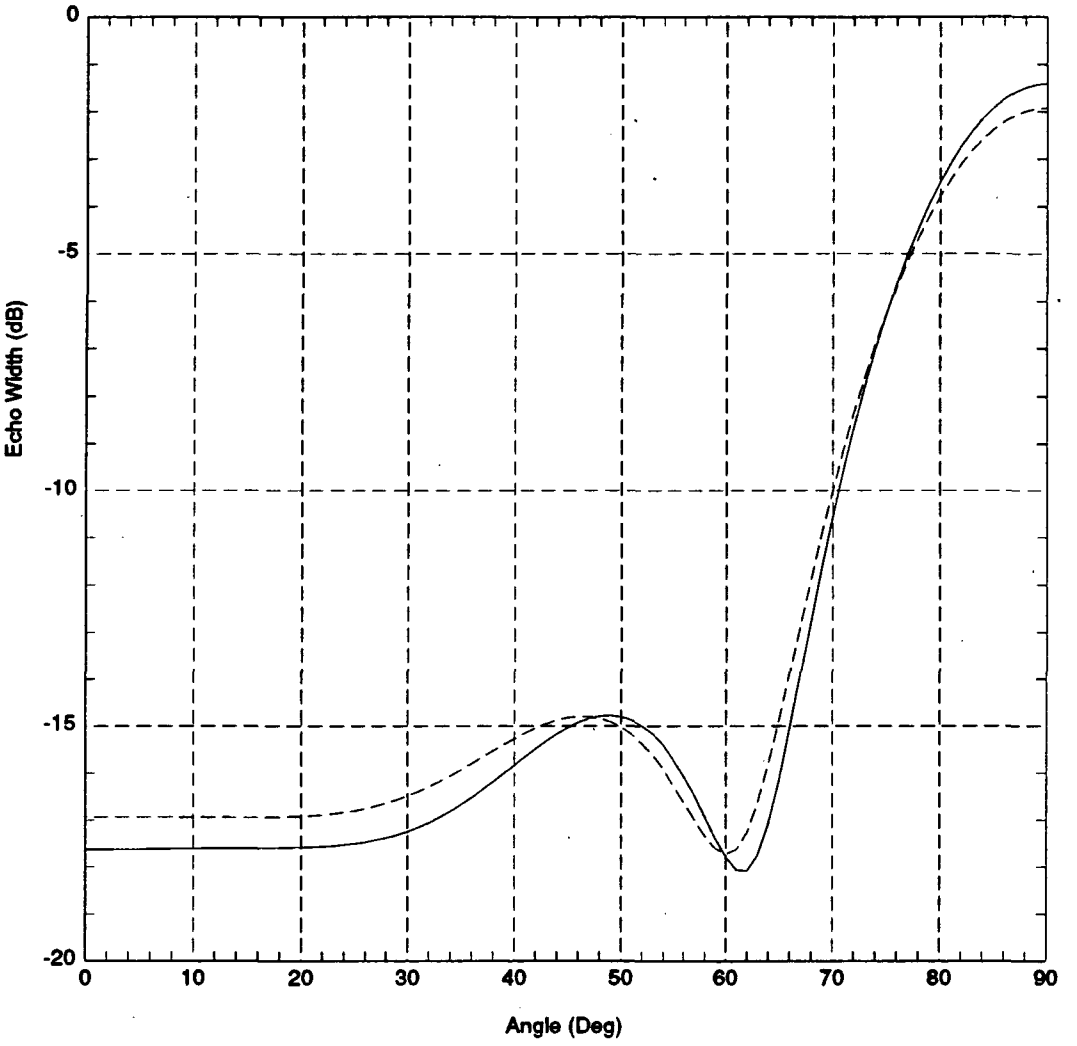

Figure 3.6: TM bistatic echo width for the flat strip. FEM/BEM - solid, Eigenfunction - dashed.

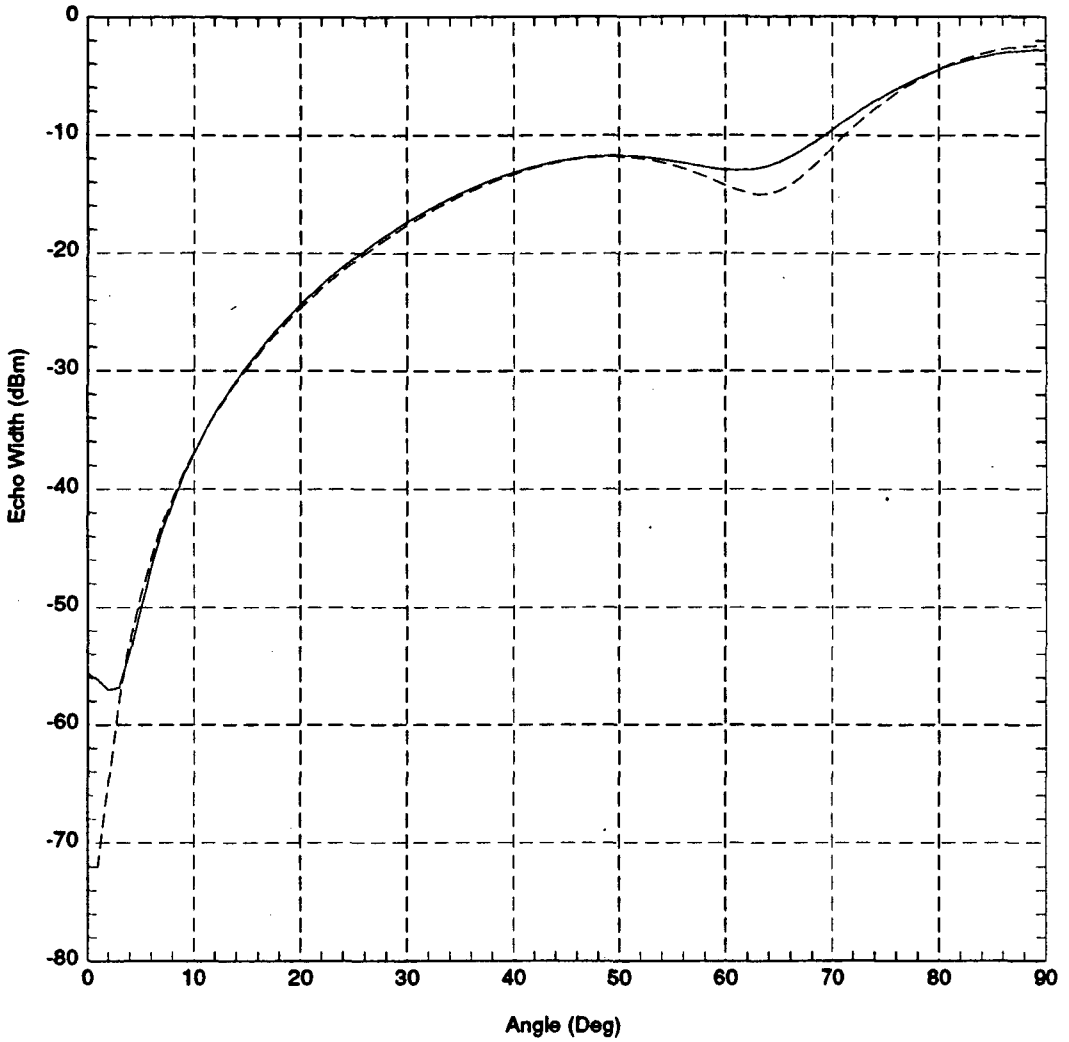

Figure 3.7: TE bistatic echo width for the flat strip. FEM/BEM - solid, Eigenfunction - dashed.

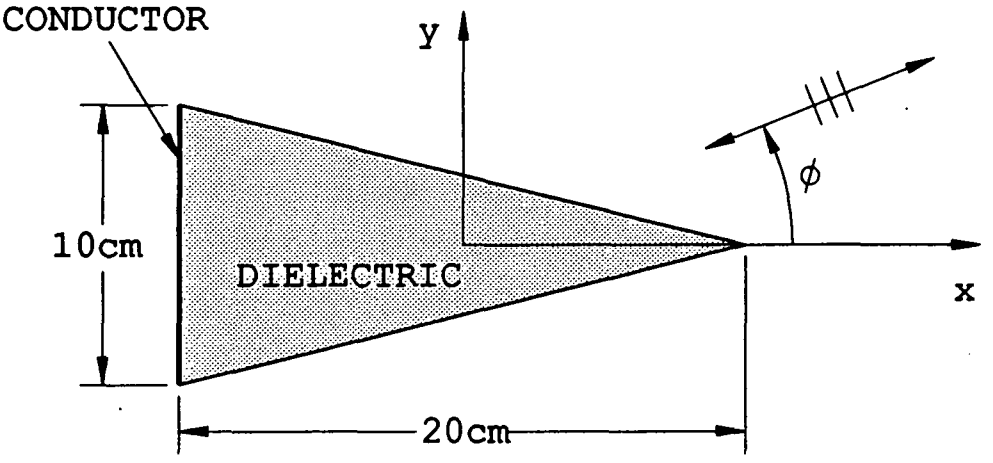

(a)

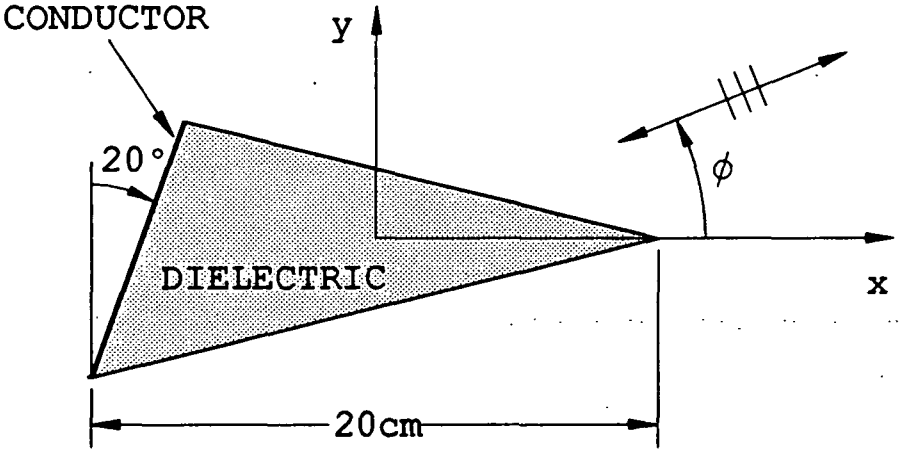

(b)

Figure 3.8: Test terminations. (a) Terminations T1 and T2, (b) Termination T3.

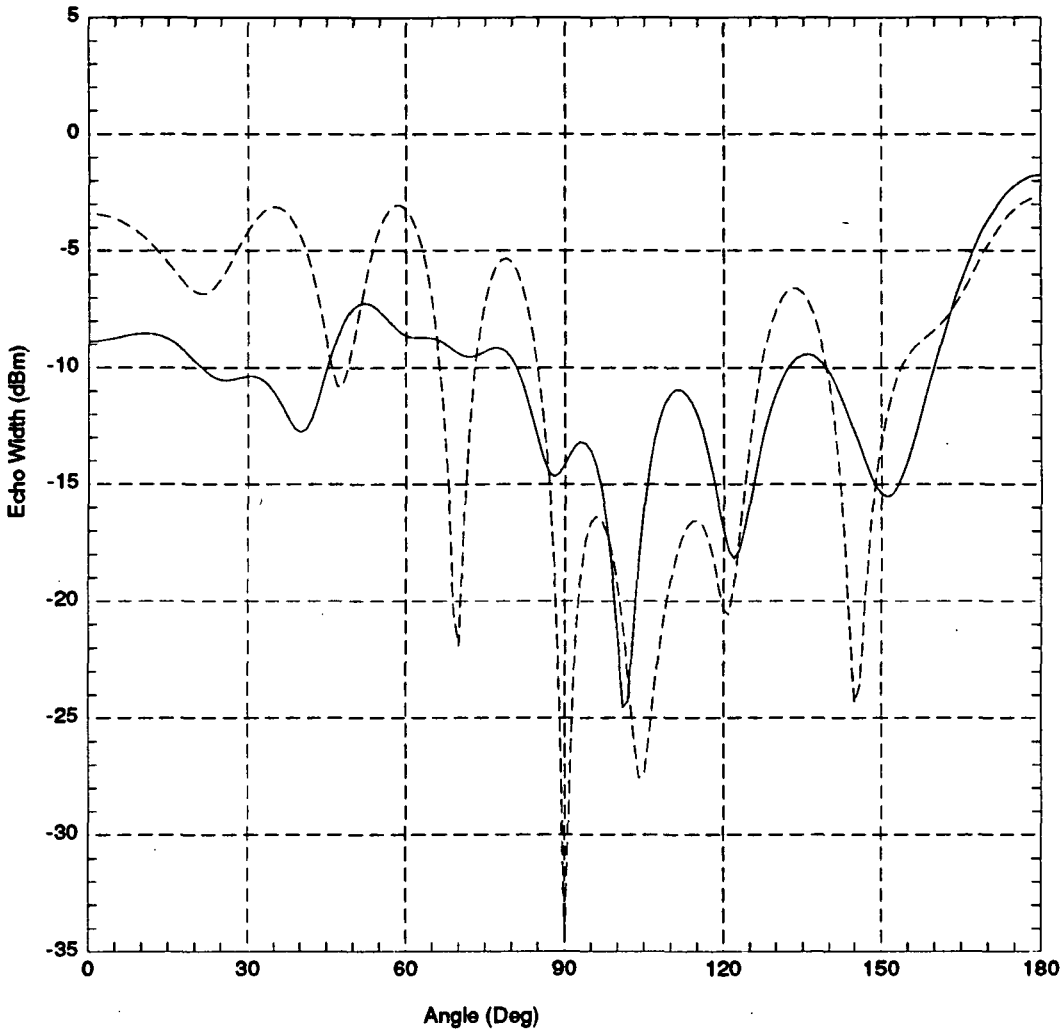

Figure 3.9: Echo widths for termination T1. TM - solid, TE - dashed.

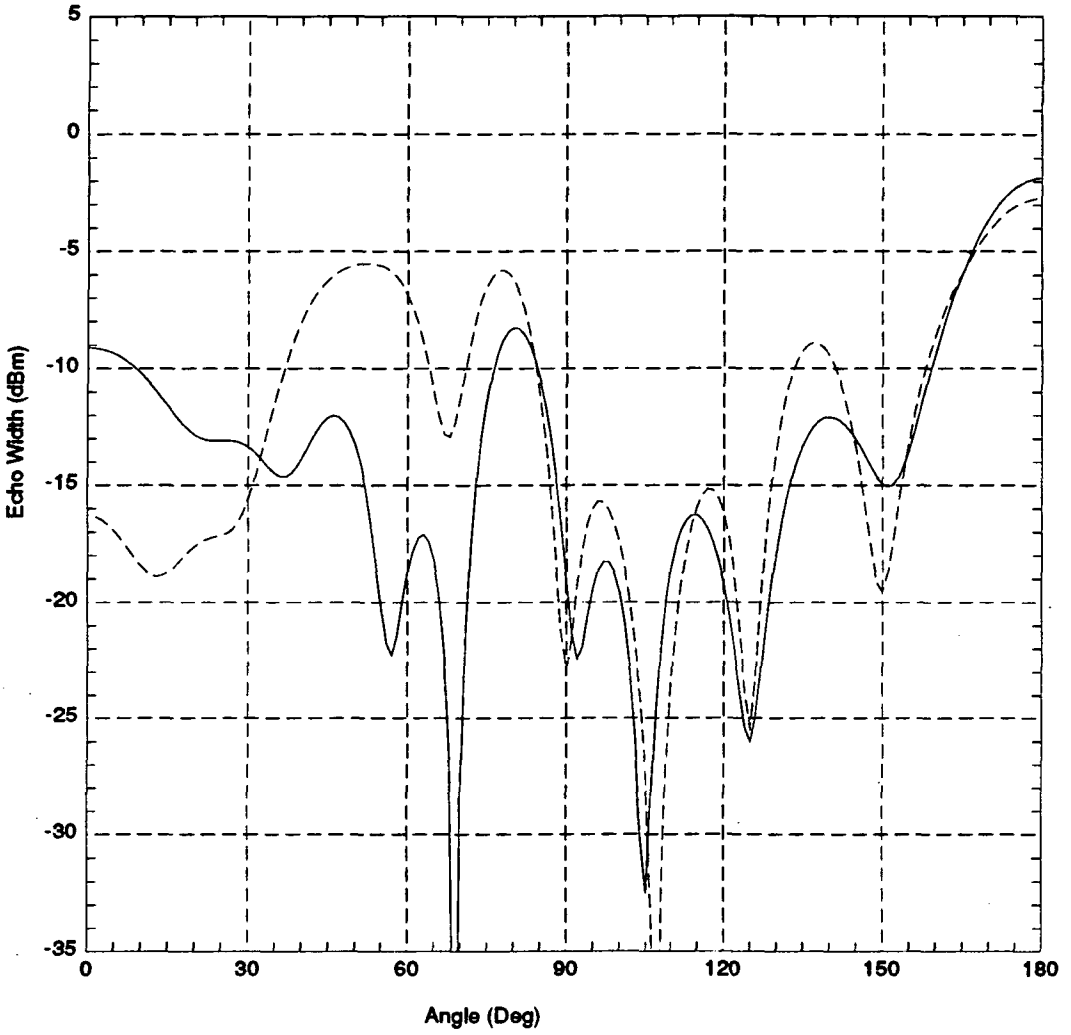

Figure 3.10: Echo widths for termination T2. TM - solid, TE - dashed.

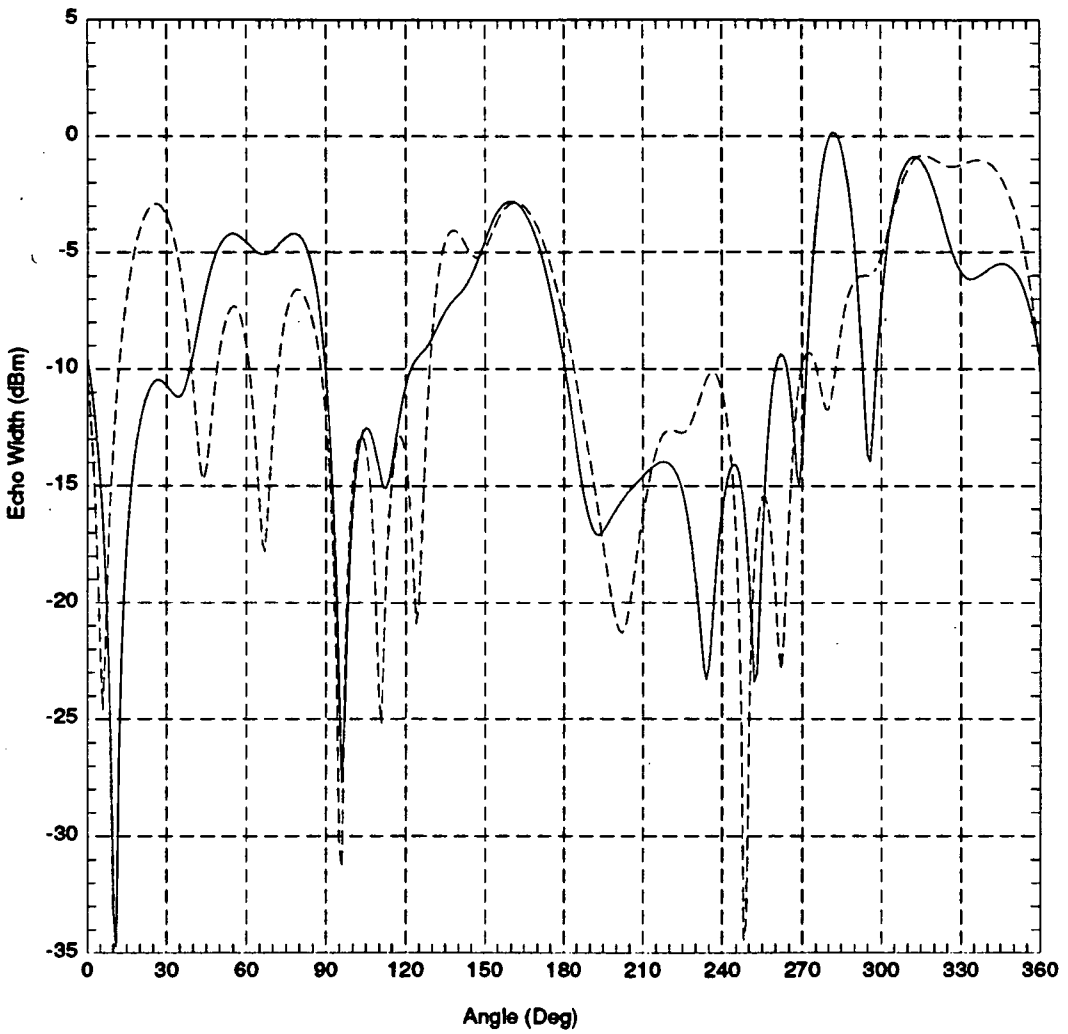

Figure 3.11: Echo widths for termination T3. TM - solid, TE - dashed.

A final plot is shown in Figure 3.12 which illustrates the internal TE scattered fields for termination T3 at an incidence angle of 25°. This angle was chosen due to the large echo width return, however, the correlation between near field distribution and echo width value is not simple. This plot does illustrate the standing wave pattern from waves due to localized scattering centers. These scattering centers can conceptually be identified by tracking the standing wave nature for a geometry when its electrical size is sufficiently large. The benefit of knowing these locations is that appropriate action can be taken to treat them from a scattering viewpoint.

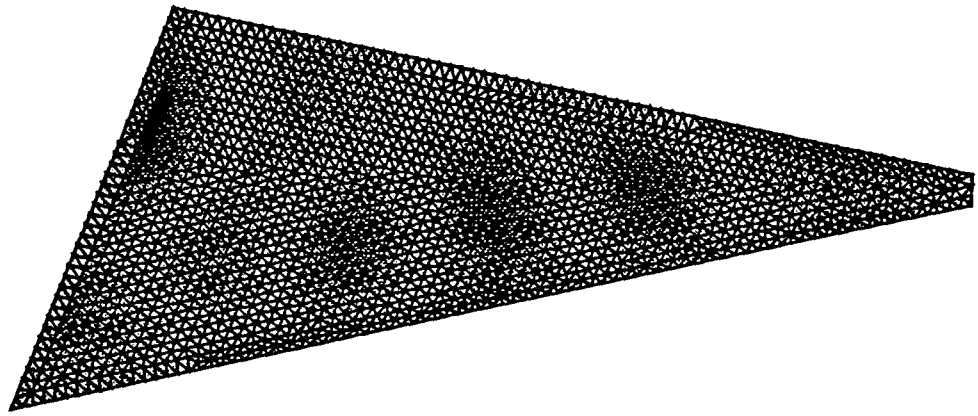

Figure 3.12: The internal TE scattered field for termination T3 with illumination from 25°.

Chapter 4

Conclusions

The status of a computer code for the calculation of the electromagnetic scattering for two dimensional geometries is presented. The code is based upon a finite element (FEM) solution for a bounded region. Two different approaches are examined to extend the solution for an unbounded region. One is using an absorbing boundary condition to simulate a reflectionless boundary (ABC) and the other one couples interior and exterior fields at a boundary through an integral equation (BEM). The advantages of the present FEM/BEM approach is that 1) no field approximations are made as in the ABC approach, 2) the boundary is placed at the outer contour of the geometry which minimizes the FEM unknowns and 3) this particular FEM/BEM approach, unlike others, retains the full advantage of the sparseness associated with the FEM interior region for matrix inversion.

Future activities include both the refinement of the existing code and the study of particular terminations of interest using both numerical and experimental approaches.

Appendix A

BEM/FEM Numerical Implementation

I Introduction

This appendix will consider in more detail the calculation of the matrices $M_{jk}^{\psi+}$, $M_{jk'}^{\phi+}$ and the vector V_j used in the FEM-BEM. The relationship of V_j to the far field calculation will also be outlined.

II Geometry

The boundary for the FEM-BEM is defined by the mesh used in the FEM solution. This consists of a set of geometry nodes connected by line segments. The line segments form the boundary elements. Let the number of geometry nodes, which equals the number of boundary elements, be N_g. Figure A.1 shows a boundary with $N_g = 5$. The boundary elements are indexed such that element number e is between geometry nodes e and $(e \bmod N_g)+1$. The following discussion for the boundary element implementation includes both linear and quadratic generating functions.

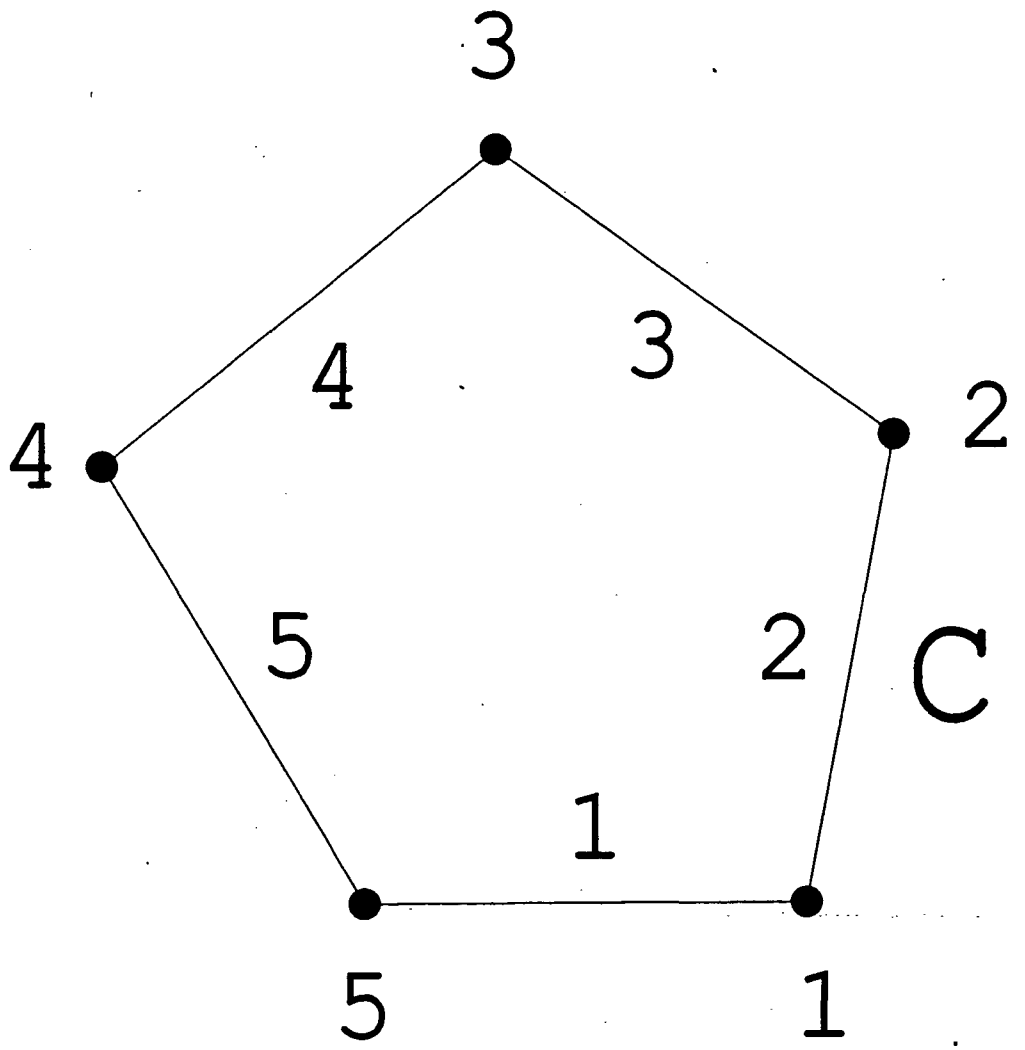

Figure A.1: A five sided boundary. The numbering of the nodes and boundary elements is shown.

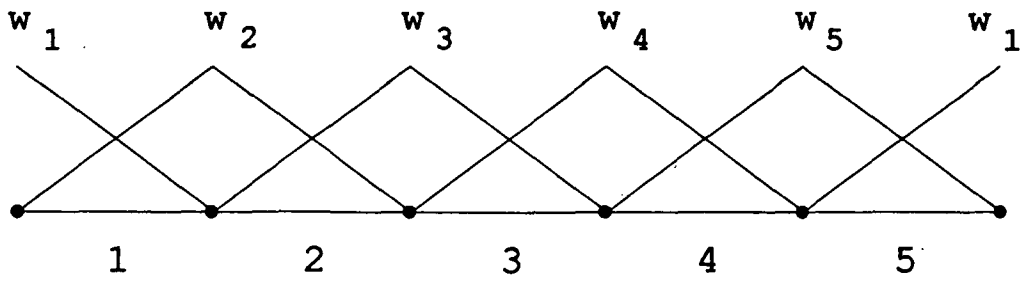

Figure A.2: Linear generating functions on the boundary elements.

For linear generating functions, the boundary nodes used as the unknowns for the FEM-BEM are the same as the geometry nodes, $N_B = N_g$. Consider the set of linear generating functions for Figure A.1 as shown in Figure A.2. The generating functions are combinations of the elemental linear functions $N^2_{e,i}$ $(i = 1,2; \mathrm{e} = 1, N_g)$ defined on each boundary element e as,

$$N^2_{e,1}(\xi) = 1 - \xi \tag{A.1}$$

$$N^2_{e,2}(\xi) = \xi \tag{A.2}$$

where ξ is a normalized distance along the element $(0 < \xi < 1)$. For example, the linear generating function w_4 is given by,

$$w_4 = N^2_{3,2} + N^2_{4,1}. \tag{A.3}$$

For any linear generating function k,

$$w_k = N^2_{((k-2) \bmod N_g + 1),2} + N^2_{k,1}. \tag{A.4}$$

This formula gives the subscripts of $N^2_{e,i}$ as a function of k. The inverse relationship is also useful. Each function $N^2_{e,i}$ is a part of exactly one generating function w_k. For linear elements, the *kth* boundary generating function which has $N^2_{e,i}$ as part of its expansion is

$$\begin{array}{rcll} k & = & \mathrm{e} & (i = 1) \\ k & = & (e \bmod N_g) + 1 & (i = 2) \end{array} \tag{A.5}$$

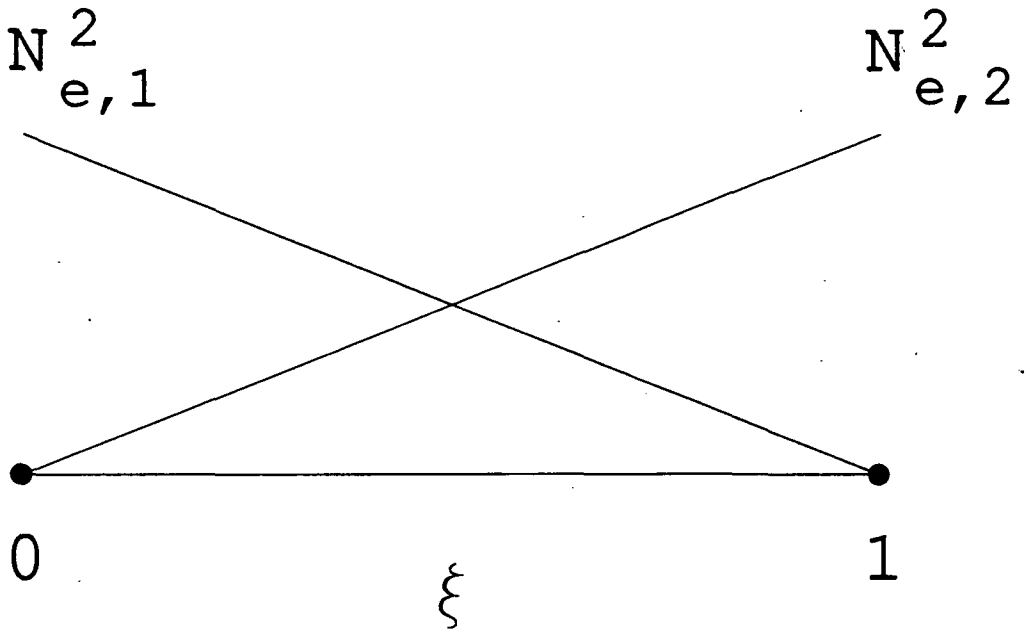

Figure A.3: Elemental linear generating functions on a single boundary element.

The set of quadratic generating functions for Figure A.1 is shown in Figure A.4. The interior boundary nodes are shown as open circles. The numbers correspond to the boundary elements. These generating functions are combinations of the elemental quadratic functions $N^3_{e,i}$ $(i = 1,3; e = 1, N_g)$. The three functions $N^3_{e,i}$ defined on boundary element e are,

$$N^3_{e,1}(\xi) = 2\xi^2 - 3\xi + 1 \qquad \text{(A.6)}$$

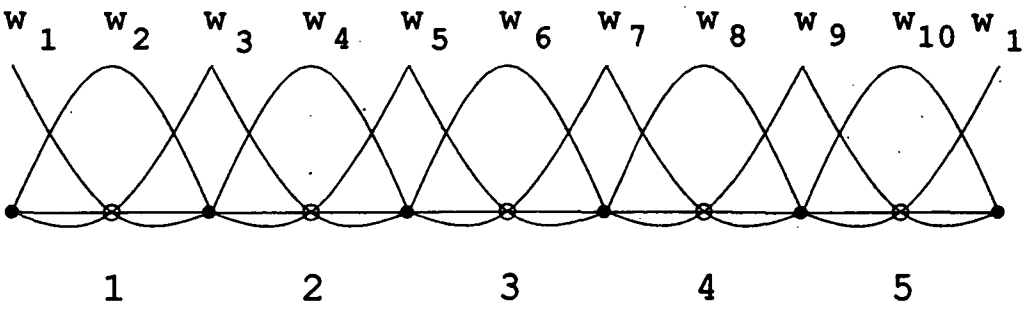

Figure A.4: Quadratic generating functions on the boundary elements.

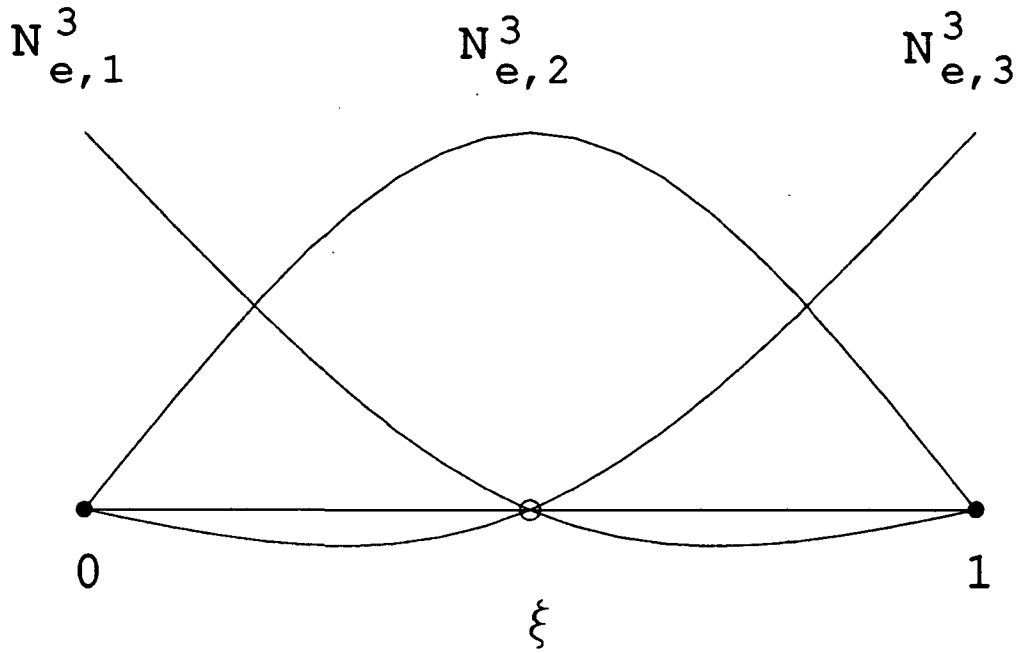

Figure A.5: Elemental quadratic generating functions on a single boundary element.

$$N^3_{e,2}(\xi) = -4\xi^2 + 4\xi \tag{A.7}$$

$$N^3_{e,3}(\xi) = 2\xi^2 - \xi \tag{A.8}$$

where ξ is again the normalized distance along the boundary element ($0 < \xi < 1$). The expansion of w_j on the set of functions $N^3_{e,i}$ depends on whether j is even (an internal node) or odd (a geometry node),

$$w_{2j'} = N^3_{j',2} \tag{A.9}$$

$$w_{2j'-1} = N^3_{((j'-2) \bmod N_g+1),3} + N^2_{j',1} \tag{A.10}$$

for $j' = 1, N_g$. Notice that $w_{2j'}$ extends over one boundary element while $w_{2j'-1}$ extends over two. Each function $N^3_{e,i}$ is a part of exactly one quadratic generating function. The *kth* quadratic boundary function which has $N^3_{e,i}$ as part of its expansion is

$$\begin{array}{lll} k = 2e-1 & (i=1) \\ k = 2e & (i=2) \\ k = 2(e \bmod N_g)+1 & (i=3). \end{array} \tag{A.11}$$

The matrices $M_{jk}^{\psi+}$ and $M_{jk'}^{\phi+}$ are defined by,

$$M_{jk}^{\psi+} = \nu^+ \int_C \int_C w_j^B(\vec{\rho}) G_0(\vec{\rho}, \vec{\rho}') w_k^B(\vec{\rho}') dl' dl \tag{A.12}$$

$$M_{jk'}^{\phi+} = \int_C w_j^B w_{k'}^B dl - \int_C \int_C w_j^B(\vec{\rho}) \frac{\partial G_0(\vec{\rho}, \vec{\rho}')}{\partial n'} w_{k'}^B(\vec{\rho}') dl' dl. \tag{A.13}$$

The actual integrations will be done over the functions $N_{e,i}^p$ and $N_{f,n}^p$ resulting in the terms

$$m_{f,n;e,i}^{\psi+} = \nu^+ \int_C \int_C N_{f,n}^p(\xi) G_0(\vec{\rho}, \vec{\rho}') N_{e,i}^p(\xi') dl' \tag{A.14}$$

$$m_{f,n;e,i}^{\phi+} = \int_C N_{f,n}^p(\xi) N_{e,i}^p(\xi) dl - \int_C \int_C N_{f,n}^p(\xi) \frac{\partial G_0(\vec{\rho}, \vec{\rho}')}{\partial n'} N_{e,i}^p(\xi') dl' dl. \tag{A.15}$$

These integrals are defined over straight line elements. For a given pair of boundary elements e and f, the integrals for $(i = 1, p)$ and $(j = 1, p)$ can be done simultaneously thus saving run time in function calls for the Green's function. The terms $m_{f,n;e,i}^{\psi+}$ and $m_{f,n;e,i}^{\phi+}$ are added to the appropriate matrix elements of $M_{jk}^{\psi+}$ and $M_{jk'}^{\phi+}$ based on the formulas in Equations (A.5) or (A.11).

The voltage vector V_j is defined as

$$V_j = \int_C w_j^B \phi_{inc} dl'. \tag{A.16}$$

The integrals

$$v_{e,i} = \int_C N_{e,i}^p(\xi') \phi_{inc} dl' \tag{A.17}$$

are calculated for each boundary element e with $(i = 1, N_g)$ and combined to form the V_j vector.

The following notation and assumptions will be made for the BEM integrations. The integral around the boundary will be done in a counterclockwise direction. This defines the integration path along each boundary element. Let $\vec{\rho}_e$ be the position of the geometry node of boundary element e where the integral begins. The vector from one end point to the other is $\vec{l}_e$ where $l_e = \| \vec{l}_e \|$ is the length of boundary element e. Any point on the boundary element is given by

$$\vec{\rho} = \vec{\rho}_e + \xi \vec{l}_e \tag{A.18}$$

for $0 < \xi < 1$. The outward normal and the exterior region will always be to the right of the integration path. The outward unit normal is then given by

$$\hat{n}_e = \left(\vec{l}_e \times \hat{z}\right) / l_e. \tag{A.19}$$

III Component $m^{\psi+}_{f,n;e,i}$

The free space Green's function for the two dimensional wave equation is,

$$G_0(\vec{\rho}, \vec{\rho}') = \frac{-j}{4} H_0^{(2)}(k \| \vec{\rho} - \vec{\rho}' \|). \tag{A.20}$$

Using this Green's function in Equation (A.14) for the term $m^{\psi+}_{f,n;e,i}$ and parameterizing the line integrals with Equation (A.18) gives,

$$m^{\psi+}_{f,n;e,i} = \frac{-j l_e l_f}{4} \int_0^1 \int_0^1 N^p_{f,n}(\xi) N^p_{e,i}(\xi') H_0^{(2)}(k \| \vec{\rho} - \vec{\rho}' \|) d\xi' d\xi \tag{A.21}$$

$$\vec{\rho} = \vec{\rho}_f + \vec{l}_f \xi \tag{A.22}$$

$$\vec{\rho}' = \vec{\rho}_e + \vec{l}_e \xi' \tag{A.23}$$

$$\vec{\rho} - \vec{\rho'} = (\vec{\rho}_f - \vec{\rho}_e) + (\vec{l}_f \xi - \vec{l}_e \xi'). \tag{A.24}$$

From the symmetry of this integral,

$$m^{\psi+}_{e,i;f,n} = m^{\psi+}_{f,n;e,i}. \tag{A.25}$$

This means that we only need to do a calculation of $m^{\psi+}_{f,n;e,i}$ for $e \leq f$. The symmetry gives all the cases for $e > f$.

The Hankel function of order zero has a logarithmic singularity at $\| \vec{\rho} - \vec{\rho'} \| = 0$. When elements e and f are separated, the integrand is well behaved and a simple Gaussian quadrature is sufficient to calculate the double integral. When elements e and f touch at an endpoint, there is one logarithmic singular point in the unit square of ξ, ξ' space where the integration is done. This is a very mild singularity and can be ignored when a Gaussian quadrature is used.

When $e = f$, the logarithmic singularity becomes a line ($\xi = \xi'$) in the unit square. This double integral must be done more carefully to get accurate answers. For $e = f$,

$$m^{\psi+}_{f,n;e,i} = \frac{-jl_e l_f}{4} \int_0^1 N^p_{f,n}(\xi) \left\{ \int_0^1 N^p_{e,i}(\xi') H_0^{(2)}(kl_e \mid \xi - \xi' \mid) d\xi' \right\} d\xi. \tag{A.26}$$

The innermost integral will be examined. It has the form,

$$\{\} = \int_0^1 f(\xi') d\xi' \tag{A.27}$$

$$= \int_0^\xi f(\xi') d\xi' + \int_\xi^1 f(\xi') d\xi' \tag{A.28}$$

where $f(\xi')$ has a log singularity at $\xi' = \xi$. The singularity will be moved to zero in the integration variable with the transformation $t = \frac{\xi - \xi'}{\xi}$ in the first integral and $t = \frac{\xi' - \xi}{1-\xi}$ in the second,

$$\{\} = \int_0^1 \xi f(\xi(1-t)) + (1-\xi) f(\xi + (1-\xi)t)\, dt. \tag{A.29}$$

Substituting the integrand of the double integral for $f(\xi')$,

$$\begin{aligned} \{\} &= \int_0^1 \xi N_{e,i}^p(\xi(1-t))\, H_0^{(2)}(kl_e\xi t) \\ &\quad + (1-\xi) N_{e,i}^p(\xi + (1-\xi)t)\, H_0^{(2)}(kl_e(1-\xi)t)\, dt. \end{aligned} \tag{A.30}$$

Let $N_{e,i}^p(x) = a_2x^2 + a_1x + a_0$. This equation works for linear ($p = 2$) or quadratic ($p = 3$) functions. Then,

$$N_{e,i}^p(\xi(1-t)) = t^2 a_2\xi^2 + t(-a_1\xi - 2a_2\xi^2) + (a_0 + a_1\xi + a_2\xi^2) \tag{A.31}$$

$$\begin{aligned} N_{e,i}^p(\xi + (1-\xi)t) &= t^2 a_2(1-\xi)^2 + t\left(a_1(1-\xi) + 2a_2\xi(1-\xi)\right) \\ &\quad + (a_0 + a_1\xi + a_2\xi^2). \end{aligned} \tag{A.32}$$

Substituting this expansion in powers of the integration variable t into Equation (A.30) gives,

$$\begin{aligned} \{\} = \xi & \left\{ a_2\xi^2 I_2(kl_e\xi) - (a_1\xi + 2a_2\xi^2) I_1(kl_e\xi) \right. \\ & \left. + (a_0 + a_1\xi + a_2\xi^2) I_0(kl_e\xi) \right\} \\ + (1-\xi) & \left\{ a_2(1-\xi)^2 I_2\left(kl_e(1-\xi)\right) \right. \\ & + \left(a_1(1-\xi) + 2a_2\xi(1-\xi)\right) I_1\left(kl_e(1-\xi)\right) \\ & \left. + (a_0 + a_1\xi + a_2\xi^2) I_0\left(kl_e(1-\xi)\right) \right\} \end{aligned} \tag{A.33}$$

where the $I_k(\alpha)$ are defined as

$$I_k(\alpha) = \int_0^1 \eta^k H_0^{(2)}(\alpha\eta) d\eta. \tag{A.34}$$

The reduction of these integrals was done in [8, 11] and is repeated here.

Not much can be done with $I_0(\alpha)$ except integrate the series expansion of $H_0^{(2)}$,

$$H_0^{(2)}(z) = J_0(z) - jY_0(z) \tag{A.35}$$

$$J_0(z) = \sum_{k=0}^{\infty} \frac{(-1)^k}{(k!)^2} \left(\frac{z^2}{4}\right)^k \tag{A.36}$$

$$Y_0(z) = \frac{2}{\pi}\left(\ln\left(\frac{z}{2}\right) + \gamma\right) J_0(z) - \frac{2}{\pi} \sum_{k=1}^{\infty} \frac{(-1)^k}{(k!)^2} \left(\frac{z^2}{4}\right)^k \sum_{s=1}^{k} \frac{1}{s} \tag{A.37}$$

where $\gamma = .57721\ldots$ is Euler's constant. Grinding through the integral gives

$$\int_0^z H_0^{(2)}(z')dz' = z \sum_{k=0}^{\infty} \frac{(-1)^k}{(k!)^2} \left(\frac{z^2}{4}\right)^k \frac{1}{2k+1} \cdot \left[1 - j\frac{2}{\pi}\left\{\ln(\frac{z}{2}) + \gamma - \frac{1}{2k+1} - \sum_{s=1}^{k} \frac{1}{s}\right\}\right] \tag{A.38}$$

$$I_0(\alpha) = \frac{1}{\alpha} \int_0^{\alpha} H_0^{(2)}(z')dz'. \tag{A.39}$$

The last summation is defined to be zero when $k = 0$, $\sum_{s=1}^{0} \frac{1}{s} = 0$. The integral for $I_1(\alpha)$ can be done exactly,

$$I_1(z;\alpha) \equiv \int_0^z \eta H_0^{(2)}(\alpha\eta)d\eta \tag{A.40}$$

$$= \frac{1}{\alpha} \int_0^z \frac{d}{d\eta}\left(\eta H_1^{(2)}(\alpha\eta)\right) d\eta \tag{A.41}$$

$$= \frac{\eta}{\alpha} H_1^{(2)}(\alpha\eta). \tag{A.42}$$

Using the small argument approximation of $H_1^{(2)}(\alpha\eta)$ at $\eta \approx 0$ gives,

$$I_1(\alpha) = \frac{1}{\alpha}\left[H_1^{(2)}(\alpha) - \frac{2j}{\pi\alpha}\right]. \tag{A.43}$$

$I_2(\alpha)$ is found by an integration by parts,

$$\begin{aligned} I_2(z;\alpha) &\equiv \int_0^z \eta^2 H_0^{(2)}(\alpha\eta)d\eta && \text{(A.44)} \\ &= \int_0^z \eta I_1'(\eta;\alpha)d\eta && \text{(A.45)} \\ &= \eta I_1(\eta;\alpha)\mid_0^z - \int_0^z I_1(\eta;\alpha)d\eta && \text{(A.46)} \\ &= \eta I_1(\eta;\alpha)\mid_0^z + \frac{1}{\alpha^2}\int_0^z \eta \frac{d}{d\eta}\left(H_0^{(2)}(\alpha\eta)\right)d\eta && \text{(A.47)} \\ &= \eta I_1(\eta;\alpha)\mid_0^z + \frac{1}{\alpha^2}\left[\eta H_0^{(2)}(\alpha\eta)\mid_0^z - \int_0^z H_0^{(2)}(\alpha\eta)d\eta\right] && \text{(A.48)} \end{aligned}$$

$$I_2(\alpha) = \frac{1}{\alpha}H_1^{(2)}(\alpha) + \frac{1}{\alpha^2}H_0^{(2)}(\alpha) - \frac{1}{\alpha^2}I_0(\alpha). \qquad \text{(A.49)}$$

The $e = f$ term is evaluated by doing a Gaussian quadrature on the outer integral in Equation (A.26). For each value of ξ, the inner integral is evaluated using Equation (A.33) and the $I_k(\alpha)$ functions given above.

IV Component $m^{\phi+}_{f,n;e,i}$

The normal derivative of the free space Green's function is,

$$\begin{aligned} \frac{\partial G_0(\vec{\rho},\vec{\rho'})}{\partial n'} &= \hat{n'}\cdot\nabla G_0(\vec{\rho},\vec{\rho'}) \\ &= \frac{-jk}{4}H_1^{(2)}(k \parallel \vec{\rho}-\vec{\rho'} \parallel)\hat{n'}\cdot\hat{R} && \text{(A.50)} \end{aligned}$$

where $\hat{R}$ is a unit vector from the source to the field point,

$$\hat{R} = (\vec{\rho}-\vec{\rho'})/ \parallel \vec{\rho}-\vec{\rho'} \parallel . \qquad \text{(A.51)}$$

When $e = f$, there is a singularity in the second integral in Equation (A.15) for $m^{\phi+}_{f,n;e,i}$. This singularity comes from the $\frac{1}{\|\vec{\rho}-\vec{\rho'}\|}$ behavior of the Hankel function of order one. Also, with $e = f$ on a linear path of integration, $\hat{n'}\cdot\hat{R} =$

0 except at $\vec{\rho} = \vec{\rho'}$. The net effect of the second integral in Equation (A.15) is to reduce the first integral by one half resulting in,

$$\begin{aligned} m^{\phi+}_{e,n;e,i} &= \frac{1}{2}\int_C N^p_{e,n}(\xi)N^p_{e,i}(\xi)dl \\ &= \frac{l_e}{2}\int_0^1 N^p_{e,n}(\xi)N^p_{e,i}(\xi)d\xi. \end{aligned} \tag{A.52}$$

This integral can be done exactly which gives

$$\int_0^1 N^2_{e,1}(\xi)N^2_{e,1}(\xi)d\xi = \int_0^1 N^2_{e,2}(\xi)N^2_{e,2}(\xi)d\xi = \frac{1}{3} \tag{A.53}$$

$$\int_0^1 N^2_{e,1}(\xi)N^2_{e,2}(\xi)d\xi = \frac{1}{6} \tag{A.54}$$

for linear generating functions and

$$\int_0^1 N^3_{e,1}(\xi)N^3_{e,1}(\xi)d\xi = \int_0^1 N^3_{e,3}(\xi)N^3_{e,3}(\xi)d\xi = \frac{2}{15} \tag{A.55}$$

$$\int_0^1 N^3_{e,2}(\xi)N^3_{e,2}(\xi)d\xi = \frac{8}{15} \tag{A.56}$$

$$\int_0^1 N^3_{e,1}(\xi)N^3_{e,2}(\xi)d\xi = \int_0^1 N^3_{e,3}(\xi)N^3_{e,2}(\xi)d\xi = \frac{1}{15} \tag{A.57}$$

$$\int_0^1 N^3_{e,1}(\xi)N^3_{e,3}(\xi)d\xi = \frac{-1}{30} \tag{A.58}$$

for quadratic generating functions.

When $e \neq f$, Equation (A.15) reduces to,

$$m^{\phi+}_{f,n;e,i} = \frac{jkl_el_f}{4}\int_0^1\int_0^1 N^p_{f,n}(\xi)N^p_{e,i}(\xi')H^{(2)}_1(k \parallel \vec{\rho} - \vec{\rho'} \parallel)(\hat{n'_e}\cdot\hat{R})d\xi'd\xi. \tag{A.59}$$

$$\vec{\rho} = \vec{\rho}_f + \vec{l}_f\xi \tag{A.60}$$

$$\vec{\rho'} = \vec{\rho}_e + \vec{l}_e\xi' \tag{A.61}$$

$$\vec{\rho} - \vec{\rho'} = (\vec{\rho}_f - \vec{\rho}_e) + (\vec{l}_f\xi - \vec{l}_e\xi'). \tag{A.62}$$

In general $m^{\phi+}_{f,n;e,i} \neq m^{\phi+}_{e,i;f,n}$ because of the term $(\hat{n'_e}\cdot\hat{R})$. However, by calculating both $(\hat{n'_e}\cdot\hat{R})$ and $(\hat{n'_f}\cdot\hat{R})$, both terms $m^{\phi+}_{f,n;e,i}$ and $m^{\phi+}_{e,i;f,n}$ can be calculated in the same integration loop.

For $e \neq f$ and e not touching f, the integrand of Equation (A.59) is well behaved and can be found by a simple Gaussian quadrature.

When $e \neq f$ and e touches f at a corner, there is a singularity at that corner. While this singularity is not severe, it can be easily removed. We assume $f = e \bmod N_g + 1$ so that $\vec{\rho}_f = \vec{\rho}_e + \vec{l}_e$. Let $\eta = 1 - \xi'$ $(d\eta = -d\xi')$ in Equation (A.59),

$$\begin{aligned} m^{\phi+}_{f,n;e,i} &= \frac{jkl_el_f}{4}\int_0^1\int_0^1 N^p_{f,n}(\xi)N^p_{e,i}(1-\eta) \\ &\quad H^{(2)}_1(k \parallel \vec{\rho} - \vec{\rho}' \parallel)(\hat{n}'_e \cdot \hat{R})d\eta d\xi. \qquad \text{(A.63)} \\ \vec{\rho} &= \vec{\rho}_f + \vec{l}_f\xi \qquad \text{(A.64)} \\ \vec{\rho}' &= \vec{\rho}_f - \vec{l}_e\eta \qquad \text{(A.65)} \\ \vec{\rho} - \vec{\rho}' &= (\vec{l}_f\xi + \vec{l}_e\eta). \qquad \text{(A.66)} \end{aligned}$$

The double integral over the unit square in ξ,η space is divided into two triangular regions as shown in Figure A.6,

$$m^{\phi+}_{f,n;e,i} = m^{upper}_{f,n;e,i} + m^{lower}_{f,n;e,i}. \qquad \text{(A.67)}$$

For the lower triangle, let $\xi = t$, $\eta = th$. This gives

$$\begin{aligned} m^{lower}_{f,n;e,i} &= \frac{jkl_el_f}{4}\int_0^1\int_0^1 N^p_{f,n}(t)N^p_{e,i}(1-th)\cdot \\ &\quad \cdot H^{(2)}_1(k \parallel \vec{\rho} - \vec{\rho}' \parallel)(\hat{n}'_e \cdot \hat{R})tdtdh \qquad \text{(A.68)} \\ \vec{\rho} - \vec{\rho}' &= t(\vec{l}_f + \vec{l}_e h). \qquad \text{(A.69)} \end{aligned}$$

Notice how the singularity at $t = 0$ has been removed since the term $tH^{(2)}_1(k \parallel \vec{\rho} - \vec{\rho}' \parallel)$ is bounded at $t = 0$. For the upper triangle, let $\eta = s$, $\xi = sw$. This gives

$$\begin{aligned} m^{upper}_{f,n;e,i} &= \frac{jkl_el_f}{4}\int_0^1\int_0^1 N^p_{f,n}(sw)N^p_{e,i}(1-s) \\ &\quad H^{(2)}_1(k \parallel \vec{\rho} - \vec{\rho}' \parallel)(\hat{n}'_e \cdot \hat{R})sdsdw \qquad \text{(A.70)} \\ \vec{\rho} - \vec{\rho}' &= s(\vec{l}_e + \vec{l}_f w). \qquad \text{(A.71)} \end{aligned}$$

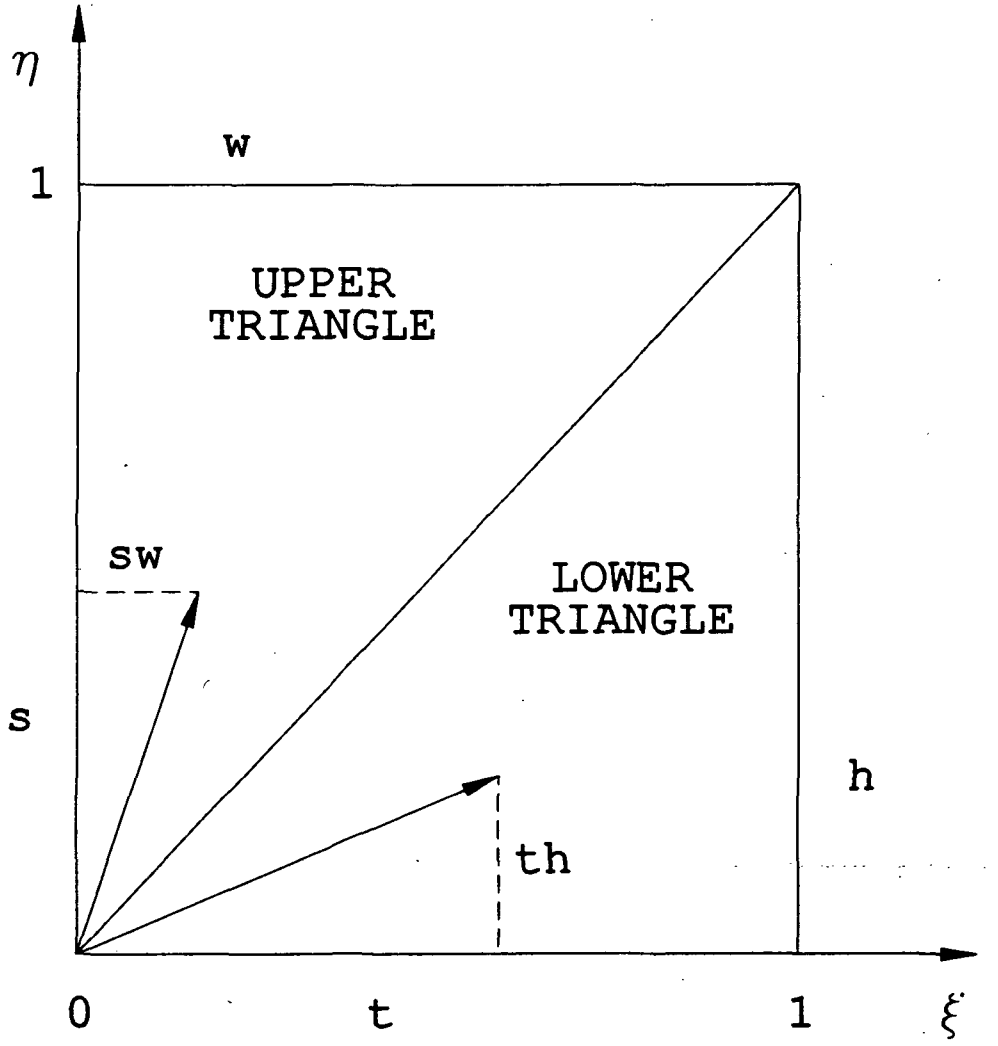

Figure A.6: The division of the unit square into upper and lower triangles.

The singularity at $s = 0$ has been removed. Since the integrands for $m^{upper}_{f,n;e,i}$ and $m^{lower}_{f,n;e,i}$ are well behaved, a Gaussian quadrature is used for the double integrals. Adding the results as in Equation (A.67) gives $m^{\phi+}_{f,n;e,i}$ for the case $e < f$ and touching. The case $e > f$ and touching is found by calculating the two terms $m^{\phi+}_{f,n;e,i}$ and $m^{\phi+}_{e,i;f,n}$ simultaneously as indicated earlier.

V Component $v_{e,i}$

The induced voltage depends on the incident field. We assume here that the incident field is a plane wave of unit magnitude coming from the $\hat{\rho}_{inc}$ direction,

$$\phi_{inc} = e^{-j\vec{k}_{inc}\cdot\vec{\rho}} \tag{A.72}$$

$$= e^{jk_0\hat{\rho}_{inc}\cdot\vec{\rho}}. \tag{A.73}$$

Equation (A.17) gives the term $v_{e,i}$,

$$v_{e,i} = l_e \int_0^1 N^p_{e,i}(\xi) e^{jk_0\hat{\rho}_{inc}\cdot(\vec{\rho}_e+\vec{l}_e\xi)} d\xi \tag{A.74}$$

$$= l_e e^{jk_0\hat{\rho}_{inc}\cdot\vec{\rho}_e} \int_0^1 N^p_{e,i}(\xi) e^{ja\xi} d\xi \tag{A.75}$$

$$a = k_0\hat{\rho}_{inc}\cdot\vec{l}_e. \tag{A.76}$$

Substituting the polynomial expansion $N^p_{e,i}(\xi) = a_2\xi^2 + a_1\xi + a_0$ into this equation gives,

$$v_{e,i} = A_e\left(a_2 J_2(a) + a_1 J_1(a) + a_0 J_0(a)\right) \tag{A.77}$$

$$A_e = l_e e^{jk_0\hat{\rho}_{inc}\cdot\vec{\rho}_e} \tag{A.78}$$

$$J_k(a) = \int_0^1 \xi^k e^{ja\xi} d\xi. \tag{A.79}$$

The $J_k(a)$ integrals can be reduced,

$$J_0(a) = \frac{1}{ja}\left(e^{ja} - 1\right) \tag{A.80}$$

$$J_1(a) = \frac{1}{ja}\left(e^{ja} - J_0(a)\right) \tag{A.81}$$

$$J_2(a) = \frac{1}{ja}\left(e^{ja} - 2J_1(a)\right) \tag{A.82}$$

for $a \neq 0$. For a close to or equal to zero, the $J_k(a)$ integrals are best evaluated using the series expansion for $e^{ja\xi}$,

$$J_k(a) = \sum_{l=0}^{\infty} \frac{(ja)^k}{l!\,(k+l+1)!}. \tag{A.83}$$

VI Far Field

The far field ϕ_{far} in the $\hat{\rho}_{far}$ direction in terms of the boundary fields $\phi_{k'}$, ψ_k at the nodal points is,

$$\begin{aligned}\phi_{far}(\hat{\rho}_{far}\rho) = \frac{e^{-jk_0\rho}}{\sqrt{\rho}}\left(\frac{j}{4}\sqrt{\frac{2j}{\pi k_0}}\right)\Bigg[&\sum_{k=1}^{N_B}\psi_k\nu^+\int_C w_k^B(\vec{\rho}')e^{jk_0\hat{\rho}_{far}\cdot\vec{\rho}'}dl' \\ &+\sum_{k'=1}^{N_B}\phi_{k'}\int_C -jk_0(\hat{n}'\cdot\hat{\rho}_{far})w_{k'}^B(\vec{\rho}')e^{jk_0\hat{\rho}_{far}\cdot\vec{\rho}'}dl'\Bigg].\end{aligned} \tag{A.84}$$

This can be written as,

$$\phi_{far}(\hat{\rho}_{far}\rho) = \frac{e^{-jk_0\rho}}{\sqrt{\rho}}C\left(\psi_k F_k^{\psi} + \phi_{k'}F_{k'}^{\phi}\right) \tag{A.85}$$

$$F_k^{\psi} = \int_C w_k^B(\vec{\rho}')e^{jk_0\hat{\rho}_{far}\cdot\vec{\rho}'}dl' \tag{A.86}$$

$$F_{k'}^{\phi} = \int_C -jk_0(\hat{n}'\cdot\hat{\rho}_{far})w_{k'}^B(\vec{\rho}')e^{jk_0\hat{\rho}_{far}\cdot\vec{\rho}'}dl' \tag{A.87}$$

$$C = \left(\frac{j}{4}\sqrt{\frac{2j}{\pi k_0}}\right) \tag{A.88}$$

where an implicit summation over repeated indices has been used. Here again, the terms

$$F^{\psi}_{e,i} = l_e \int_0^1 N^p_{e,i}(\xi') e^{jk_0 \hat{\rho}_{far} \cdot \vec{\rho'}} d\xi' \tag{A.89}$$

$$F^{\phi}_{e,i} = -jk_0(\hat{n'} \cdot \hat{\rho}_{far}) l_e \int_0^1 N^p_{e,i}(\xi') e^{jk_0 \hat{\rho}_{far} \cdot \vec{\rho'}} d\xi' \tag{A.90}$$

are calculated for each boundary element e $(i = 1, p)$ and combined to give F^{ψ}_{k}, $F^{\phi}_{k'}$. The factor $(\hat{n'} \cdot \hat{\rho}_{far})$ is constant over the linear boundary element e and so it was removed from the integrand.

By comparing the far field Equations (A.89) and (A.90) with the voltage Equation (A.74), the far field terms $F^{\psi}_{e,i}$, $F^{\phi}_{e,i}$ can be written as,

$$F^{\psi}_{e,i} = A'_e \left(a_2 J_2(a') + a_1 J_1(a') + a_0 J_0(a')\right) \tag{A.91}$$

$$F^{\phi}_{e,i} = -jk_0(\hat{n'} \cdot \hat{\rho}_{far}) A'_e \left(a_2 J_2(a') + a_1 J_1(a') + a_0 J_0(a')\right) \tag{A.92}$$

where A'_e and a' are defined by

$$A'_e = l_e e^{jk_0 \hat{\rho}_{far} \cdot \vec{\rho}_e} \tag{A.93}$$

$$a' = k_0 \hat{\rho}_{far} \cdot \vec{l}_e. \tag{A.94}$$

The $J_k(a)$ functions were defined earlier.

Bibliography

[1] M. Kragalott and E. Newman, "A User's Manual for the General Cylinder Code (GCYL)," Technical Report 722644-1, ElectroScience Laboratory, The Ohio State University, June 1990; prepared for Rosemount, Inc, Burnsville, MN, under Contract No. PO D55951.

[2] P. Silvester and R. Ferrari, Finite Element for Electrical Engineers, 2nd Edition, 1990 Cambridge University Press.

[3] B. McDonald and A. Wexler, "Finite-Element Solution of Unbounded Field Problems," *IEEE Trans. Microwave Theory Tech.*, Vol. MTT-20, pp. 841-847, Dec. 1972.

[4] Structural Research and Analysis Corporation, 1661 Lincoln Blvd, Suite 200 Santa Monica, CA, 90404.

[5] A. Bayliss and E. Turkel, "Radiation Boundary Conditions for Wavelike Equations," *Comm. Pure Appl. Math*, Vol. 33, pp. 707-725, 1980.

[6] D.J. Richards, A. Wexler, "Finite-Element Solutions within Curved Boundaries," *IEEE Transactions on Microwave Theory and Techniques*, Vol. MTT-20, No. 10, October 1972.

[7] J, Yashiro and S. Ohkawa, "Boundary Element Method for Electromagnetic Scattering from Cylinders," *IEEE Antennas Prop.*, Vol. AP-33, No. 4, pp. 383-389, April 1985.

[8] A. Cangellaris and R. Lee, "The Bimoment Method for Two Dimensional Electromagnetic Scattering," *IEEE Antennas Prop.*, Vol. AP-38, No. 9, pp. 1429-1436, Sept. 1990.

[9] K. Wu, G. Delisie, D. Fang, M. LeCours, "Coupled Finite Element and Boundary Element Methods in Electromagnetic Scattering,", Finite Element and Finite Difference Methods in Electromagnetic Scattering, Ed. M. Morgan, Elsevier Science Publishing Co., 1990.

[10] J. Jin and V. Liepa, "Application of Hybrid Finite Element Method to Electromagnetic Scattering From Coated Cylinders," *IEEE Antennas Prop.*, Vol. AP-36, No. 1, pp. 50-54, Jan. 1988.

[11] M. Koshiba and M.Suzuki, "Application of the Boundary-Element Method to Waveguide Discontinuities," *IEEE Microwave Theory Tech.*, Vol. MTT-34, No. 2, pp. 301-307, 1986.

[12] R. Collins, "Bandwidth Reduction by Automatic Renumbering," *International Journal for Numerical Methods in Engineering*, Vol. 6, pp. 345-356, 1973.

723224-3, "Analysis of Lossy Composite Terminating Structures" Andre, Dominek, Munk and Wang, September 1991